University of Nevada, Reno

Achieving Near-Natural Locomotion in Transfemoral Amputees - A Control Theoretic Approach

A dissertation submitted in partial fulfillment of the

requirements for the degree of Doctor of Philosophy in

Electrical Engineering

by

Zunaed Kibria

Dr. Sesh Commuri/Dissertation Advisor

May 2024

THE GRADUATE SCHOOL

We recommend that the thesis
prepared under our supervision
by

Zunaed Kibria

entitled

Achieving Near-Natural Locomotion in Transfemoral Amputees - A Control Theoretic Approach

be accepted in partial fulfillment of the
requirements for the degree of

Doctor of Philosophy

Sesh Commuri, Ph.D.

Advisor

Jeongwon Park, Ph.D.

Committee Member

Hao Xu, Ph.D.

Committee Member

Yantao Shen, Ph.D.

Committee Member

Jun Zhang, Ph.D.
Graduate School Representative

Markus Kemmelmeier, Ph.D., Dean
Graduate School

May 2024

ABSTRACT

Amputation of the lower limb is prescribed to address conditions such as trauma, vascular issues, tumors, neuropathy, frostbite, and complications from diabetes. Post-surgery, the individual has to be fitted with a prosthetic limb to regain mobility. While a good-fitting, well-designed prosthetic device can help support body weight and locomotion, the loss of lower limb muscles profoundly impacts body support, and stability and often results in asymmetrical gait patterns.

Traditionally, prosthetic limbs were designed primarily to support weight and mimic the appearance of natural limbs. However, modern prosthetic devices aim for active functionality, striving to replicate near-natural human locomotion. However, achieving such functionality is not an easy task as the control of the prosthetic limb has to determine the user's intent while adapting to unknown nonlinear dynamics, and varying terrain and environmental conditions.

Among lower limb amputations, transtibial amputations are the most common. The loss of the ankle joint for transtibial amputees causes several constraints during gait, such as lower walking speed, increased metabolic energy expenditure, and reduced power in the amputated limb during the push-off phase. For above-knee amputations, where the individual loses both the knee and ankle joints, the effects are more severe. Losing multiple joints leads to significant asymmetry in gait, which can affect musculoskeletal health in the long run.

This dissertation addresses the critical challenges encountered in controlling above-knee prosthetic limbs to promote a symmetrical gait and natural movement in transfemoral amputees. Traditional control methods often fall short due to the inherent uncertainty in user intent and prosthetic dynamics. To overcome these limitations, two intelligent controllers are designed for above-knee prostheses.

A pivotal component of this dissertation is a comparative case study conducted to analyze muscle activity and gait asymmetry in individuals with osteomyoplastic transfemoral amputation (OTFA) compared to able-bodied counterparts. The findings reveal significant muscle activity in residual muscles during various gait types among OTFA subjects, emphasizing notable asymmetries in their gait patterns. This empirical insight underscores the critical need to address gait asymmetry in both prosthetic limb design and control strategies.

A radial basis function neural network-based controller has been designed and developed to reduce gait asymmetry. The controller showed significant improvement from the traditional PD controller which is mostly used for prosthetic leg systems. The designed controller is stable and shows promising results in optimizing the gait asymmetry cost function.

The second intelligent control strategy for the prosthetic leg is a novel neuro-dynamic approach, leveraging actor-critic networks to learn and adapt control actions dynamically. The primary objective is to minimize long-term gait asymmetry between the intact and amputated sides, thereby enabling a gait closer to natural human locomotion. Stability analysis confirms the method's robustness and its capacity to adapt to varying user gaits.

Further validation through numerical simulations and Monte Carlo analysis underscores the controller's efficacy across diverse dynamics and user requirements.

By synthesizing findings from the proposed control strategies and the empirical case study, this dissertation significantly contributes to the advancement of prosthetic limb technology and rehabilitation practices for transfemoral amputees. It is known that, minimizing gait asymmetry not only enhances user safety but also reduces metabolic energy consumption and musculoskeletal strain. Moreover, it mitigates the risk of long-term health issues such as cardiovascular complications associated with persistent asymmetrical gait patterns.

In conclusion, this dissertation presents a comprehensive analysis and control approach dedicated to achieving natural human locomotion in transfemoral amputees. Through innovative control strategies and empirical studies, it sheds light on the complexities of gait asymmetry and offers practical solutions to enhance prosthetic limb functionality and user well-being. Moving forward, continued research efforts should explore and refine these approaches to further improve the mobility and overall quality of life for individuals with above-knee amputations.

To the people who work to alleviate suffering and improve the lives of others.

ACKNOWLEDGMENTS

First and foremost, I extend my sincere gratitude to my advisor Dr. Sesh Commuri, for his unwavering support and invaluable guidance throughout my doctoral studies. Dr. Commuri's mentorship has not only fostered my academic growth but also empowered me to develop as an independent researcher. I am profoundly grateful for his teachings, which have instilled in me the values of perseverance and excellence, inspiring me to strive for nothing less than the best. Without his assistance, this dissertation would not have been possible.

I am thankful to the members of my dissertation committee, Dr. Jeongwon Park, Dr. Yantao Shen, Dr. Hao Xu, and Dr. Jun Zhang for their dedicated time and effort in reviewing my work and providing useful feedback. I am particularly grateful to Dr. Xu for his knowledge-sharing in the classroom and to Dr. Zhang for his enthusiastic guidance and mentorship, both inside and outside the academic sphere. Additionally, I extend my appreciation to Dr. M. Sami Fadali for his support during my tenure at UNR.

A special thanks to Bhanu Prasad Kotamraju, a former student of Dr. Commuri, whose assistance proved vitally important in several of my research projects. I also wish to acknowledge Dr. Anh Mai, another former student of Dr. Commuri, whose pioneering work provided the foundation for my dissertation. Though I have not met Dr. Mai in person, his contributions have profoundly influenced my research.

Next, I would like to thank my parents. Without their constant love, support, and sacrifices, I would not be where I am today. They worked so hard to provide me with the

best options possible. They taught me to always follow my dreams and to work hard to achieve my goals.

Finally, my deepest appreciation goes to my wife Ikra, for always being by my side. I find myself incredibly fortunate to have her in my life. Her love, sacrifices, and encouragement have helped me to stay motivated throughout this PhD journey.

Table of Contents

LIST OF TABLES

LIST OF FIGURES

Chapter 1 INTRODUCTION

1.1 Motivation

Transfemoral amputation, i.e., above-knee amputation, is often performed to address traumatic injuries, vascular deficiencies, cancerous tumors, neuroma, frostbite, or complications from diabetes [1]. The muscles in the lower limbs play a crucial role in supporting the body, facilitating movement, and maintaining stability [2]. The consequence of lower limb amputation is far-reaching and can lead to persistent health issues such as back pain, joint pain, osteoarthritis, and the manifestation of phantom limb sensations [3]. Amputation of a joint not only affects the functionality of the amputated limb but also imposes an additional workload on the remaining joints, as they compensate for the lost power [4]. It has been estimated that by the year 2050, around 3.6 million living people in the USA will have limb loss among which 18.5% will be transfemoral amputees [5].

Prosthetic legs have been commonly used to provide user support and limited mobility. However, the long-term health of an individual requires a highly mobile and active lifestyle. Such increased functionality and mobility require the prosthetic device to be fully functional, able to adapt to different terrain and gait conditions, and provide a near-natural gait. Poorly fitting, poorly functioning prosthesis not only impacts the gait of the individual but also affects the health and increases the probability of Osteoarthritis, Osteopenia, Osteoporosis, postural changes, and most commonly back pain [6].

Current prosthetic solutions, ranging from passive to active devices, are fraught

with limitations. Passive devices which act as spring or controlled damper have been used to support weight bearing of the individual [7-10]. However, users of passive devices designed for weight-bearing tend to have limited mobility and usually expend increased amounts of metabolic energy for locomotion. Semi-active prosthesis can help improve the gait of the amputee, but the performance falls short due to its inability to account for different types of gaits needed by an individual [11-14]. Active prostheses, although offering advantages like improved stability and reduced metabolic energy expenditure, often struggle with generating sufficient propulsion torque and addressing nonlinear system dynamics [15-17].

Commercially available prosthetic legs, such as Linx (Blachford), C-leg, Genium X3 (Ottobock), Rheo knee (Ossur) have been developed to support the amputee over a vast range of activities, but these systems cannot recognize and adapt to the gait of the individual. Other researchers explored the use of techniques rooted in adaptive control to improve the tracking performance of gait controllers [18-20]. However, these approaches do not address asymmetry in the gait. There are a few neural network-based learning controllers for prosthetic leg, but these are based on offline tuning policy [21-23], or limit their application to the control of one joint [24]. Recently, some researchers have developed learning based controller for both ankle and knee joints [25]. But their application is limited only to angle error optimization for self-selected gaits.

Therefore, alternative control techniques are needed for advanced prosthetic systems that not only enhance mobility but also ensure long-term health and well-being by tackling issues of adaptability by compensating nonlinear dynamics. Through a thorough

investigation of novel control strategies grounded in adaptive learning, there is potential to transform prosthetic technology and enhance the quality of life for individuals with lower limb amputations. This dissertation endeavors to delve into these innovative approaches, aiming to lay the groundwork for the development of next-generation prosthetic solutions that excel in functionality, adaptability, and user satisfaction.

1.2 Scope of the dissertation

The objective of this dissertation is to analyze the impact of transfemoral amputation on gait asymmetry and address the deficiencies observed in current prosthetic leg control systems by developing an intelligent knee-ankle joint system. The following steps have been undertaken to achieve this:

Firstly, an in-depth analysis of the effect of transfemoral amputation will be conducted. This analysis will involve studying the residual muscle activity, body weight distribution on the prosthetic device, and the impact on stance time for both legs to identify asymmetries.

Subsequently, an effective neural network learning-based controller will be designed to mitigate the challenges posed by the unknown nonlinear dynamics of the system and enhance gait symmetry.

Following that, a stable neuro-dynamic programming controller will be developed to ensure the long-term usability and effectiveness of the system.

Through these steps, this dissertation aims to contribute to the advancement of prosthetic technology by addressing key issues and laying the foundation for the creation of a more intelligent and functional knee-ankle joint system to achieve near natural gait.

1.3 Contributions of the dissertation

The following are the significant contributions of this dissertation:

a. *Establishment of test protocol:* A comprehensive test protocol is devised to gather gait data from individuals who have undergone osteomyoplastic amputation, particularly focusing on transfemoral amputees. This protocol ensures systematic data collection and forms the foundation for subsequent analyses.

b. *Analysis of gait asymmetry:* In this research, gait asymmetry has been mathematically designed as a cost function comprising knee and ankle joint tracking errors in the sagittal plane. The asymmetry function represents the difference between intact and amputated legs in terms of stance time. Through detailed analysis, the dissertation examines the asymmetry in gait patterns exhibited by transfemoral amputees compared to able-bodied individuals. This investigation sheds light on the specific challenges faced by amputees in achieving natural locomotion.

c. *Development of a neural network (NN) based controller:* A novel neural network-based controller has been developed to address gait asymmetry and promote nearly natural locomotion in transfemoral amputees. Demonstrations of the controller's stability and adaptability to varying dynamics highlight its effectiveness in improving gait symmetry. Comparative analysis reveals that the controller outperforms the classical PD controller in terms of tracking performance. Monte Carlo simulations further confirm the robustness of the designed controller across various dynamic scenarios.

d. *Implementation of a neuro-dynamic programming (NDP) based controller:* A stable neuro-dynamic programming (NDP) based controller has been developed to further reduce gait asymmetry and ensure long-term usability for individuals with transfemoral amputations. This controller offers a robust solution for sustained improvement in gait patterns, contributing to enhanced mobility and overall well-being. It outperforms classical and neural network-based controllers in terms of reducing long-term costs. Monte Carlo simulations demonstrate that under varying dynamic conditions, this controller surpasses classical PD and neural network-based controllers in reducing gait asymmetry.

Together, these contributions advance the understanding of gait asymmetry in transfemoral amputees and offer practical solutions through the development of intelligent knee-ankle joint systems. The dissertation not only addresses existing deficiencies in prosthetic leg control systems but also provides valuable insights and methodologies for improving the locomotion and quality of life of amputees.

1.4 Organization of the dissertation

The dissertation is structured as follows:

- *Chapter 2:* This chapter provides a comprehensive overview of gait analysis and muscle activity in able-bodied individuals, laying the foundation for understanding the complexities of locomotion. It also discusses a range of surgical methods for transfemoral amputations, exploring their respective merits and drawbacks.

- *Chapter 3:* In this chapter, the impact of osteomyoplastic transfemoral amputation surgery on muscle activity and stance time is examined, offering insights into the alterations in gait dynamics following the surgical procedure.
- *Chapter 4:* This chapter addresses the development of a framework for modeling and controlling prosthetic joints. The technical challenges are identified and the requirements for an intelligent knee-ankle joint system are discussed.
- *Chapter 5:* In this chapter, a cost function for quantifying gait asymmetry is defined, accompanied by the design of a stable neural network-based controller aimed at reducing asymmetry.
- *Chapter 6:* In this chapter, the design and performance of an adaptive dynamic programming-based structure, named neuro-dynamic programming controller is presented. This control approach not only reduces gait asymmetry but also ensures suitability for long-term use.

Finally, the dissertation concludes in *Chapter 7* with a summary of findings and implications, along with discussions on potential scopes for future research in the field of prosthetic joint control and gait symmetry optimization.

Chapter 2 GAIT ANALYSIS, MUSCLE ACTIVITY, AND TRANSFEMORAL AMPUTATION: A COMPREHENSIVE BACKGROUND

Gait is defined by the movement pattern of the limb while walking. Understanding the gait cycle and its sub-cycles is essential for assessing normal and pathological gait patterns, facilitating diagnosis, and guiding rehabilitation strategies for individuals with gait disorders. Analysis of these phases provides valuable insights into biomechanical abnormalities and aids in optimizing gait mechanics for improved mobility and function. Muscle contraction and joint mobility play pivotal roles in gait functionality. Any disruption in the function of leg muscles or joints can result in gait asymmetry. For various conditions, such as traumatic injuries, vascular disorders, diabetes, and tumors [29] amputation of lower limb is performed. While planning amputation, the determination of the residual limb length is dictated by patients' health and their ability to effectively use a prosthetic leg for walking [30]. Prosthetic fitting following amputation is crucial for restoring mobility and functionality, enabling users to carry out normal activities with their prosthetic limb [31]. In situations where a below-knee or transtibial amputation is not feasible, alternative options such as above-knee or transfemoral amputation may be performed [30]. In this chapter, the effects of different transfemoral amputations will be discussed.

2.1 Gait Cycle

The gait cycle is a continuous process, with one foot always in contact with the ground while the other is swinging forward. A complete gait cycle while walking can be divided into two main phases - a) stance phase and b) swing phase. This alternating pattern of stance and swing phases allows for efficient forward propulsion and balanced locomotion. Each phase is further subdivided into distinct sub-cycles, each characterized by specific biomechanical events and transitions (see Figure 2.1).

2.1.1. Stance Phase

The stance phase comprises the entire duration when a foot is in contact with the ground and can be divided into several sub-cycles based on the percentage of the gait cycle:

a. *Heel Strike (0-3%)*: Also known as initial contact, this marks the moment when the heel of the foot contacts the ground, initiating the stance phase.
b. *Loading Response / Foot Flat (3-12%)*: As the foot continues to plant on the ground, the body's weight is transferred onto it, and the foot transitions from heel strike to a flat position.
c. *Mid Stance (12-31%):* The body progresses over the planted foot, reaching a stable position as the foot moves forward and the body's center of gravity advances.
d. *Terminal Stance/ Heel off (31-50%):* As the body moves forward over the forefoot, the heel begins to lift off the ground, and the foot transitions from a pronated to a supinated position.
e. *Pre-swing / Heel Off (50-62%):* The toes push off the ground, propelling the body forward into the swing phase.

2.1.2. Swing Phase

The swing phase comprises the entire duration when a foot is off the ground and can also be divided into distinct sub-cycles based on the percentage of the gait cycle:

a. *Toe Off (62-75%):* This marks the moment when the toes leave the ground, initiating the swing phase of the gait cycle.
b. *Mid Swing (75-87%):* The swinging leg advances, reaching its maximum extension, while the knee continues to flex.
c. *Terminal Swing (87-100%):* The swinging leg prepares to make initial contact with the ground, and the knee begins to extend in preparation for the heel strike.

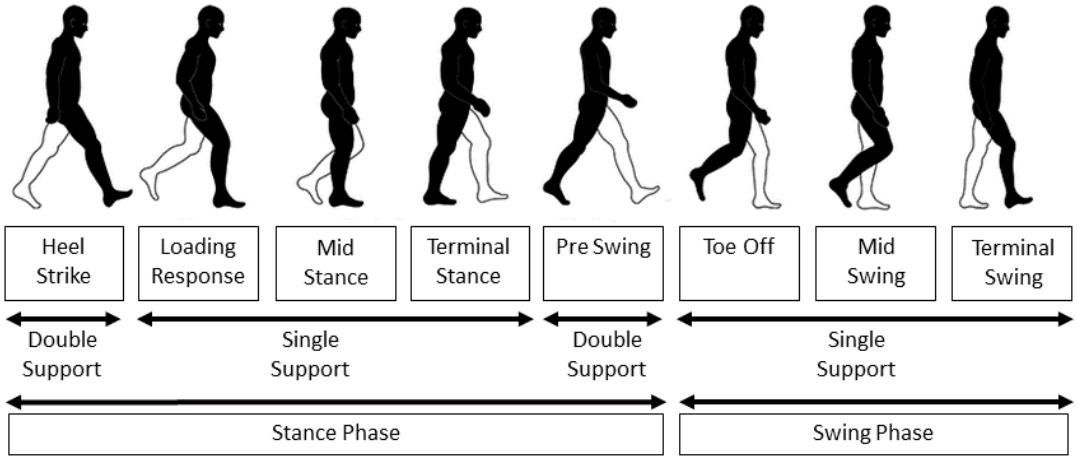

Figure 2.1: Gait cycle phases and sub-phases according to [26]. Figure recreated from [27].

2.2 Leg Muscles and Their Role in Gait

The process of walking, running, or even standing requires a sophisticated orchestration of muscles working in tandem to achieve coordinated movements. Beyond their roles in

guiding and controlling movement, these muscles also contribute to blood flow by acting as pumps. Specifically, the lower leg muscles play a crucial role in regulating and ensuring healthy blood circulation throughout the body by expanding and contracting at appropriate pressures. The anatomy of the leg muscle groups is presented in Figure 2.2.

However, the muscle groups located above the knee (Figure 2.2) are particularly instrumental in maintaining stability, generating power, and controlling movement during the gait cycle.

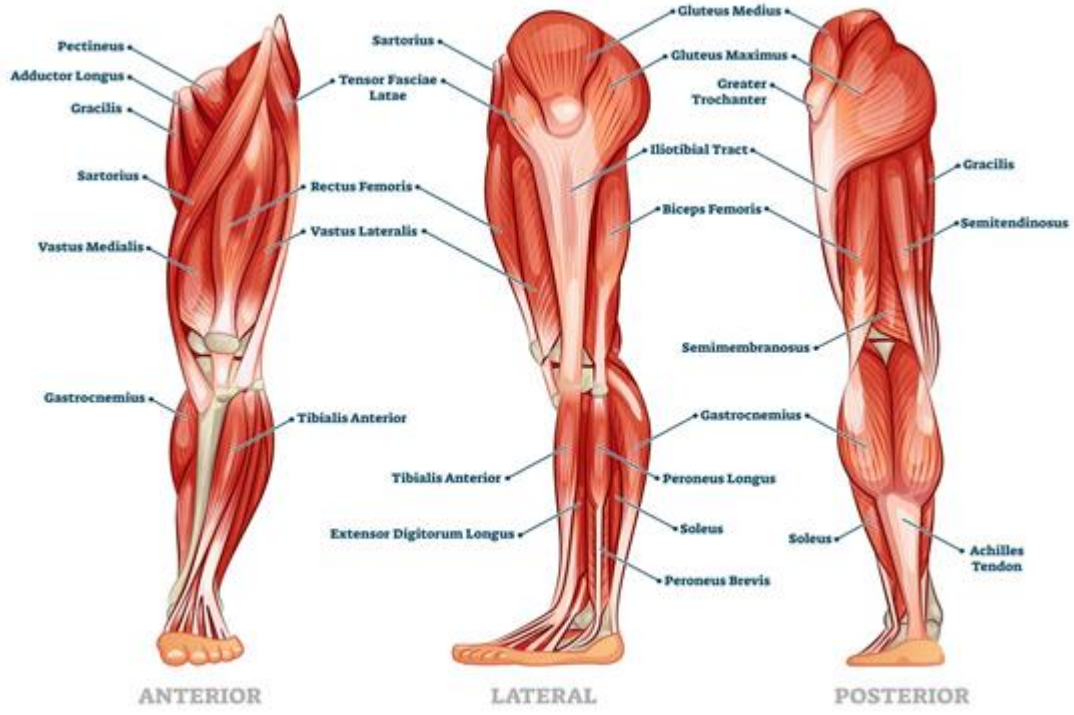

.

Figure 2.2: Leg muscle anatomical structure, labeled front, side, and back view diagrams [28].

Above knee muscle groups quadriceps, hamstrings, and adductors play pivotal role in assisting a person during a gait cycle. The function of these muscle groups is described below:

a. *Quadriceps:* The quadriceps muscle group consists of four muscles: rectus femoris, vastus intermedius, vastus lateralis, and vastus medialis. During the stance phase of the gait cycle, these muscles play a crucial role by primarily collaborating to facilitate knee joint extension. This extension action is required during the mid to terminal stance phases to support the body weight and propel the body forward. Additionally, the rectus femoris, a component of the quadriceps, has a unique role in flexing the hip joint during the swing phase. This action assists in lifting the foot off the ground and advancing the leg forward, ensuring seamless transitions between steps and preventing tripping incidents.

b. *Hamstrings:* The hamstrings muscle group comprised of biceps femoris, semitendinosus, and semimembranosus. During the swing phase, the hamstrings cause the knee joint of the leading leg to flex. This movement allows the foot to clear the ground and prepare for the next step. Furthermore, the hamstrings provide stability to the knee joint during the initial contact and loading response phases of the stance phase, ensuring smooth transitions and reducing the risk of injury.

c. *Adductors*: The adductors muscle group, which includes muscles such as the sartorius, tensor fasciae latae, pectineus, and adductor longus, significantly contributes to leg control and alignment during gait. Throughout the swing phase, these muscles stabilize the leg and prevent excessive lateral movement. By maintaining proper alignment of the lower limb, the adductors ensure coordinated movement and efficient walking mechanics.

In Figure 2.3, normalized mean EMG signals from the quadriceps, hamstring, and adductors muscle groups are presented throughout the gait cycle of a healthy able-bodied

individual. The first part of the stance phase is when the quadriceps muscles are most active. The hamstring muscles contract at the start and the finish of the gait cycle. Adductor muscles are mostly active at the start of the 'Loading Response' and 'Toe-off' phases.

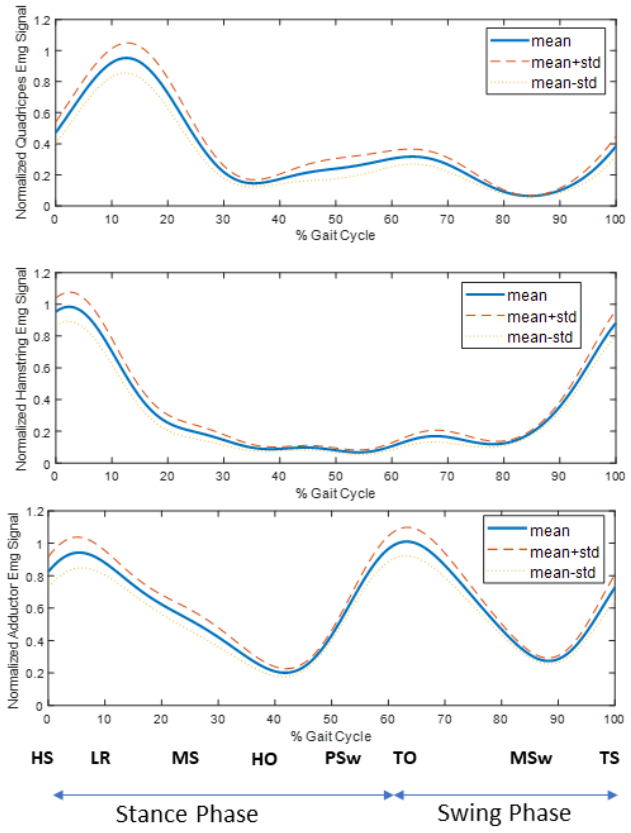

Figure 2.3: Muscle activity of Quadriceps, Hamstrings, and Adductors for an able bodied individual. HS - Heel strike, LR- Loading response, MS= Mid stance, HO – Heel off, PSw- Pre swing, TO - Toe Off, MSw – Mid Swing, TS- Terminal Swing.

2.3 Transfemoral Amputation Surgery

While performing transfemoral amputation (TFA) surgery, surgeons employ various techniques to secure muscles in the residual limb, each with its own advantages and

limitations. Two primary techniques, myodesis and myoplasty, are commonly utilized, along with emerging approaches like osseointegration (OI), aiming to enhance the functionality and quality of life for amputees.

Myodesis, predominantly employed by orthopedic surgeons, involves directly attaching dissected muscle groups to the bone [32]. After severing the femoral bone, the surgeon drills holes in the distal end and secures muscle fascia within these holes. This technique offers enhanced stability to the residual limb post-amputation. Conversely, myoplasty, performed mainly by vascular surgeons, entails bringing posterior muscles over the femur's end and stitching them to anterior muscle groups, enclosing the bone's end [33]. While myodesis is purported to provide greater stability than myoplasty, it requires meticulous surgical precision and may not be suitable for all patients. In transfemoral amputation, myodesis of the adductor tendons is a critical component of transfemoral amputation that creates dynamic muscle balance, enhances prosthetic fitting and function, and improves clinical outcomes. Traditional adductor myodesis uses locking sutures passed through cortical drill holes along the anterolateral aspect of the distal femur that are tensioned and tied by hand. In myoplasty, the surgeon brings the posterior muscles over the end of the femur and stitches them to the anterior muscle groups to enclose the end of the bone [34].

It takes around six weeks to recover from an amputation and start using prosthetic legs [36]. The proven standard for treating lower extremity amputation is the conventional socket-suspended prosthesis, which represents the interface between the transfemoral prosthetic limb and exoskeletal prosthesis. There are different techniques for designing a

socket, depending on the patient's specific requirements and anatomy. Despite advancements in socket prostheses design and materials, chronic skin problems associated with the socket remain a significant concern, affecting up to one-third of TFA patients. The friction and pressure exerted on weight-bearing areas during ambulation contribute to these issues, impacting mobility and quality of life. Osseointegration (OI) emerges as a promising solution to mitigate these challenges [37]. Originating from dentistry, OI involves anchoring the artificial limb directly into the bone (Figure 2.5). This novel technique offers several potential advantages, including direct prosthesis control, improved stability, increased walking ability, and enhanced functional capacity, ultimately leading to an improved overall quality of life.

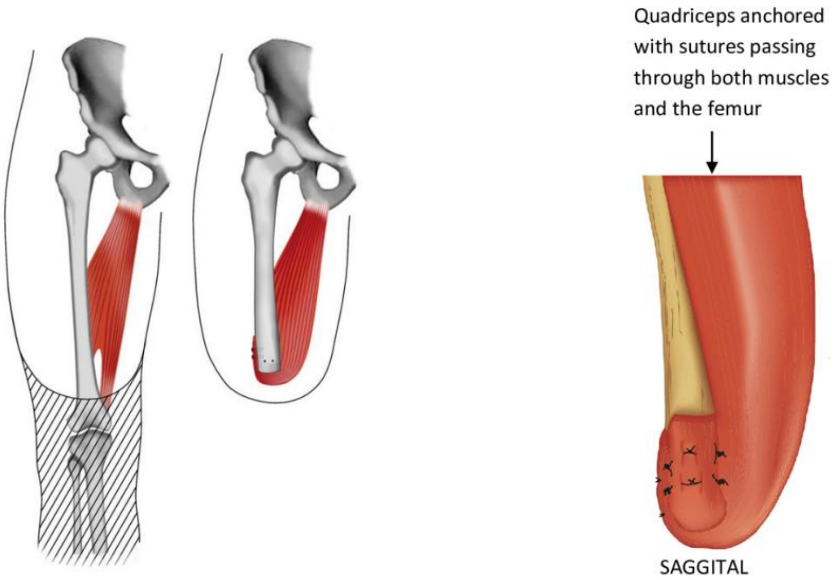

(a) (b)

Figure 2.4: a) Adductor myodesis technique. b) Myoplasty technique [35].

However, despite its advantages, osseointegration in limb amputation remains relatively novel and has some drawbacks. Reported complications include mechanical implant failure and the risk of infection [38]. The integration of foreign materials into the bone presents challenges regarding long-term stability and biocompatibility. Additionally, the cost and accessibility of osseointegration procedures may limit widespread adoption, particularly in regions with limited healthcare resources [38].

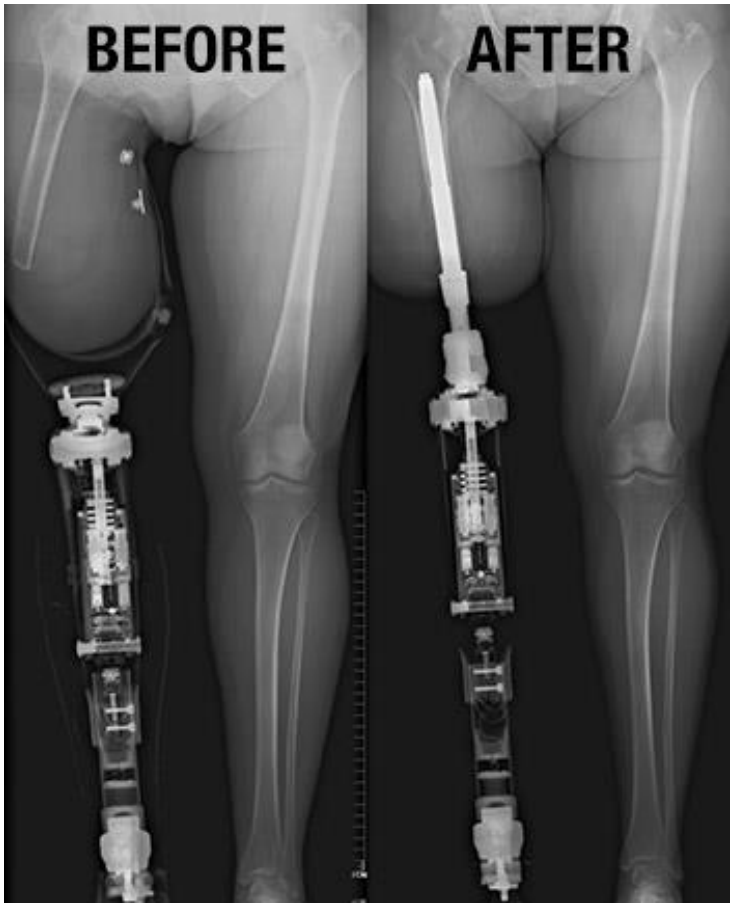

Figure 2.5: Osseointegration transfemoral amputation.

2.4 Effect of Transfemoral Amputation Surgery

Transfemoral amputation (TFA), or above-knee amputation, is a surgical procedure with profound effects on mobility, energy expenditure, physical health, and psychological well-being. Individuals who undergo TFA face numerous challenges and adaptations as they navigate life with a limb loss.

a. *Mobility and Energy Expenditure:* TFA significantly impacts walking ability, with amputees exhibiting a 30% reduced walking speed and between 30% and 60% higher energy consumption compared to able-bodied individuals. The altered gait patterns and increased hip joint range of motion result in asymmetric loading on the intact limb, leading to larger ground reaction forces and joint moments. This asymmetry may contribute to a greater risk of lower back pain and hip osteoarthritis in the intact limb.
b. *Wound Complications:* Post-amputation, individuals are at risk of various wound complications, including dehiscence, seroma, and hematoma. Factors such as sepsis, ongoing tobacco use, and higher body mass index increase the risk of these complications. However, the use of techniques like incisional negative pressure wound therapy (NPWT) has shown promise in reducing the incidence of wound complications.
c. *Phantom Limb Pain (PLP):* PLP is a common and distressing phenomenon experienced by TFA patients, characterized by sensations of pain and discomfort in the absent limb. Risk factors for PLP include pre-amputation pain, female gender, and upper or bilateral extremity amputations. A multidisciplinary approach

involving surgical techniques, analgesia, pharmacological agents, and psychotherapy is crucial for managing PLP and improving patient outcomes.

d. *Revision Amputation:* A significant proportion of TFA patients may require revision amputation procedures due to various factors such as age, crush injury, compartment syndrome, and post-surgical complications. These revisions pose additional challenges and risks for patients and require careful consideration by healthcare providers.

e. *Psychological Impact:* TFA can have a profound psychological impact on patients, leading to increased rates of depression and anxiety compared to the general population. Addressing the psychological trauma associated with limb loss is essential for promoting mental well-being and improving overall quality of life. Multimodal approaches, such as support groups and counseling programs, are emerging as effective interventions to address these psychological challenges.

f. *Muscle Function and Adaptations:* With TFA, the functionality of residual muscles is altered, leading to muscle atrophy and torque asymmetry between the amputated and intact sides. The loss of distal attachment points for muscles like the quadriceps and adductors affects their ability to generate force, further complicating mobility, and gait.

2.5 Conclusions

In conclusion, this chapter has provided a comprehensive overview of the background of gait analysis and muscle activity in an able-bodied person. By delving into the intricate

coordination of the quadriceps, hamstrings, and adductor muscles above the knee, this chapter elucidates their pivotal roles in facilitating smooth and efficient gait. Understanding these muscle functions is imperative for evaluating gait abnormalities and optimizing locomotor function. Moreover, the utilization of electromyography (EMG) signals as a primary tool for studying muscle activity underscores its significance in comprehending the dynamics of gait mechanics. This foundational knowledge lays the groundwork for subsequent chapters, offering insights into the complexities of gait analysis and muscle activity in various conditions and populations. This chapter has also highlighted the evolving surgical techniques for transfemoral amputation, aiming to overcome challenges with traditional socket prostheses. Myodesis, myoplasty, and osseointegration offer distinct approaches, each with its own benefits and limitations. While osseointegration shows promise for improved stability and function, challenges like implant failure and infection risks remain. Further research and technological advancements are crucial to optimize outcomes and ensure widespread accessibility of these innovative techniques for amputees worldwide.

Chapter 3 Effect of Osteomyoplastic Transfemoral Amputation on Residual Muscle Activation and Stance Time

3.1 Background[1]

Osteomyoplastic amputation is a commonly employed surgical procedure for transtibial cases, aimed at fostering bone growth, tissue repair, and stability in the residual limb, thus facilitating pain-free weight-bearing. This technique involves connecting the ends of the tibia and fibula to create a bony bridge, promoting vascularity, aiding in prosthetic fittings, and supporting muscle contraction during walking [39, 40]. However, in transfemoral amputation, the osteomyoplastic amputation technique differs. Following the identification of relevant anatomical structures and dissection, this procedure forms an "end cap" to surround the remaining bone instead of the construction of a bony bridge [41].

Several researchers have studied muscle activity in transfemoral amputees by concentrating on gait analysis and muscle coordination patterns. Researchers examined the gait of subjects with traditional transfemoral amputations [42-45], osseointegrated fixations [37, 46, 47], and individuals using different prostheses [48-51]. In able bodied individuals, gait and leg muscle activity analyses typically involve using electromyography (EMG) signals, often in studies related to osteoarthritis (OA) [52-55]. Though it is known from the literature that muscle activity is impacted due to amputation [48, 56], there have been no extensive studies of residual muscle activities and stance time analysis for different

[1] This chapter is adopted from "Effect of Osteomyoplastic Transfemoral Amputation on Residual Muscle Activation and Stance Time", by Zunaed Kibria, Bhanu Pasad Kotamraju, and Sesh Commuri. Submitted to 'Prosthetics and Orthotics International (POI)'

gait patterns specifically for osteomyoplastic transfemoral amputation (OTFA). To our knowledge, our study is the first to explore and compare residual muscle activity and stance time in osteomyoplastic transfemoral amputees alongside able-bodied subjects, aiming to assess gait asymmetry. In this chapter, the effects of osteomyoplastic amputation on residual limb along with intact limb will be investigated.

Figure 3.1: Osteomyoplastic amputation/ Ertl technique [41].

3.2 Objectives of the Study

Muscle activity and stance times are commonly used parameters for gait study. Hence, muscle activity and stance time in the residual and intact limbs are investigated during three types of gaits, namely, walking at a self-selected pace, walking at a brisk pace, and walking while carrying a load, encountered during normal daily activities. In all cases, the EMG signal from the residual limb is compared with the corresponding values from the intact leg to determine if the muscle activity has altered as a result of the amputation procedure. The following objectives with several research questions are posed for the study.

Objective 1: Determination of muscle activity in both legs for an osteomyoplastic transfemoral amputee.

a. Does osteomyoplastic transfemoral amputation lead to substantial muscle activity in the quadriceps, hamstring, and adductors? If so, is the muscle activity related to gait?
b. Is there a substantial difference in the muscle activity among the quadriceps, hamstring, and adductors between the intact side and the amputated side of an osteomyoplastic transfemoral amputee? If significant, is the muscle activity related to gait?

Objective 2: Determination of stance period in both legs for an able-bodied individual (ABI) and an osteomyoplastic transfemoral amputee.

a. Is there a significant difference in the stance time between the right limb and left limb of an able-bodied individual?
b. Is there a significant difference in the stance time between the intact limb and residual limb of an individual with osteomyoplastic transfemoral amputation?

Objective 3: Determination of weight loading on the prosthetic socket of an osteomyoplastic transfemoral amputee.

a. Is the weight loading on the prostheses consistent during various walking scenarios for transfemoral amputees?

Objective 4: Determination of the amputation effect of the stance time on intact limb of an osteomyoplastic transfemoral amputee.

a. Is there a significant difference between the stance times of the intact limb of an osteomyoplastic transfemoral amputation subject and the limb of an able-bodied individual?

3.3 Methods

3.3.1 Subjects

This study was approved by the Institutional Review Board at the University of Oklahoma Health Sciences Center [39]. A total of 10 men, consisting of five men with OTFA and five able-bodied intact individuals consented to participate in this research. Eligible subjects were required to be healthy and proficient in English. Able bodied subjects were capable of independently walking without any aid or assistive devices. During the study, all OTFA participants utilized their own prosthetic systems to replicate different gaits during their daily activities. A certified prosthetist supervised socket alignment and fit throughout the study. The age range of the OTFA subjects was between 23 to 38 years, while for able-bodied participants, it ranged from 24 to 40 years. Regarding physical attributes, the height and weight ranges for OTFA subjects were 69 to 74.5 inches and 131 to 220 lbs., respectively. In comparison, able-bodied subjects exhibited height and weight ranges of 70 to 78 inches and 175 to 260 lbs., respectively. The length of residual limbs for amputees ranged from 8.66 to 15.75 inches. Among the OTFA participants, four out of five underwent amputation on the right limb, with the other subject having amputation on the left limb. Detailed demographics of the subjects are tabulated in Table 3.1.

Table 3.1: Demographics of the subjects.

Subject	Amputation Type	Amputation Side	Age (Years)	Height (IN)	Weight (LBS)	Length of Residual Limb (CM)
S1	TFA	L	23	69	220	32
S2	TFA	R	38	68	192	22
S3	TFA	R	34	72	168	40
S4	TFA	R	18	69	165	30.5
S5	TFA	R	29	74.5	131	31.3
S6	N/A	N/A	24	70.5	180	N/A
S7	N/A	N/A	23	70	180	N/A
S8	N/A	N/A	27	75	175	N/A
S9	N/A	N/A	40	72	205	N/A
S10	N/A	N/A	38	78	260	N/A

3.3.2 Experimental Procedure [39]

The tests were structured to address the research questions outlined in section 3.2. The experimental procedure was designed to study the effect of OTFA on the activity of residual muscles and on the gait of the individual. To analyze the gait activities the patients were instructed to perform the following common work-related tasks:

a. *Self-selected gait (SG):* Participants were asked to walk at their own comfortable pace for 2 minutes to capture the natural gait pattern during regular walking.
b. *Brisk gait (BG):* Participants were required to walk at a brisk pace for 2 minutes to evaluate gait performance under increased speed.
c. *Weight walk (WW):* Participants were tasked with walking 25 feet while carrying a load. The load was selected carefully to ensure it did not cause excessive strain on the individual.

EMG data on muscle activity and contact force between prosthetic sockets were obtained using a Prosthetic Activity Monitor, based on an AT90USB647 microcontroller, capable of reading analog signals from 16 different channels at a frequency of 1 KHz. Eight of these channels were configured to capture force data within the prosthetic socket at 500Hz, while six channels were configured to collect EMG data from specific muscle groups (Quadriceps, Hamstrings, and Adductors) on both the intact limb and the residual limb at 1 KHz. Flexforce A201 sensors were placed within the prosthetic socket at the distal end of the residual limb to measure the contact force indicative of the end-bearing load. For intact limbs, force sensors were positioned on the ball and heel of the foot. Additionally, all subjects were equipped with a gait monitoring device (Intelligent Device for Energy Expenditure and Physical Activity - IDEEA® by MiniSun™, Fresno, CA). The force data served the dual purpose of determining gait events and synchronizing EMG signals in relation to these events. Furthermore, the force signal was used to validate the experimental data in comparison with observations from the IDEEA® system.

3.3.3 Processing EMG and Force Data

Electromyography (EMG) signals have been widely used to study muscle activity in transfemoral amputees during gait. The method described in [57] was used in this study to process the acquired EMG data. The EMG signal was rectified and filtered using a full wave rectifier and a lowpass filter with 8-Hz cutoff frequency.

To determine the root mean square (RMS) value of the EMG signal (E_{RMS}) a symmetric moving window of 150 milliseconds was used. Then, the EMG data for entire gait cycle was normalized to 100 data points and ten uniform intervals (10 data points

each). In the specific segments of the gait cycle, the mean value of E_{RMS} ($\overline{E_{RMS}}$) was determined which served as an indicator of muscle activity for that specific interval of the gait period. To analyze the muscle contraction the maximum and minimum values of $\overline{E_{RMS}}$ ($\overline{E_{RMS_{max}}}, \overline{E_{RMS_{min}}}$) were computed. To quantify the muscle activity integrated EMG (iEMG) signals were also computed for normalized EMG signal throughout the gait cycle.

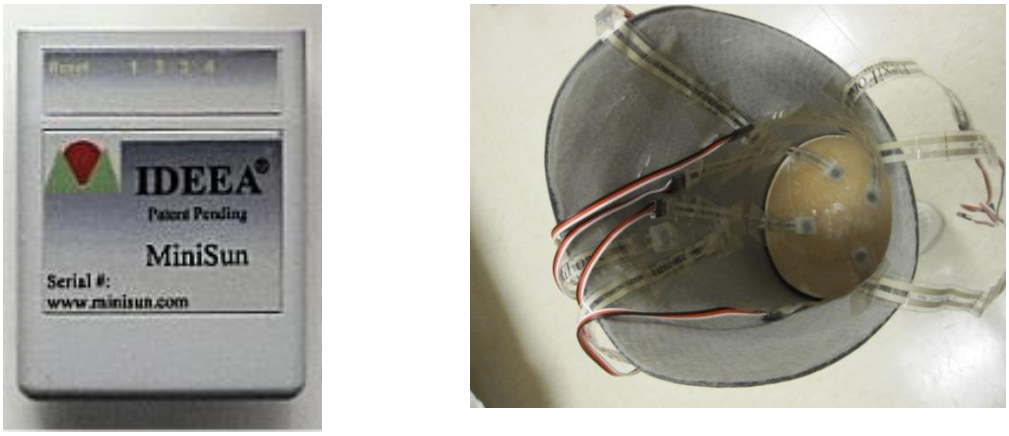

(a) (b)

Figure 3.2: (a) Gait monitoring device used in the experiment, (b) Placement of FlexiForce® sensors inside the socket.

Data from the force sensors were collected at a rate of 500 Hz through a 12-bit data acquisition board (PC-CARD-DAS16/12 AO, Measurement Computing) housed in a tablet computer carried in a backpack by the subject. The collected signals were processed, filtered with a 3 Hz cutoff frequency, and normalized to 100% of the gait cycle. Stance and swing phases were defined within each gait cycle, and peak and mean pressures during the stance phase were computed.

All the data analysis and hypothesis testing reported in this paper were done using routines implemented in MATLAB® (The MathWorks Inc, Natick, MA) [58]

3.4 Objective 1 Hypotheses: Effect on Muscle Activity for OTFA

To determine the answer of questions a, and b in Objective 1 in section 3.2, EMG data were collected, and statistical tests were performed to observe the muscle activity in both legs of the OTFA subjects. The normalized EMG signals of all three muscle groups (quadriceps, hamstring, and adductors) in a subject with osteomyoplastic amputation is shown in Figure 3.2.

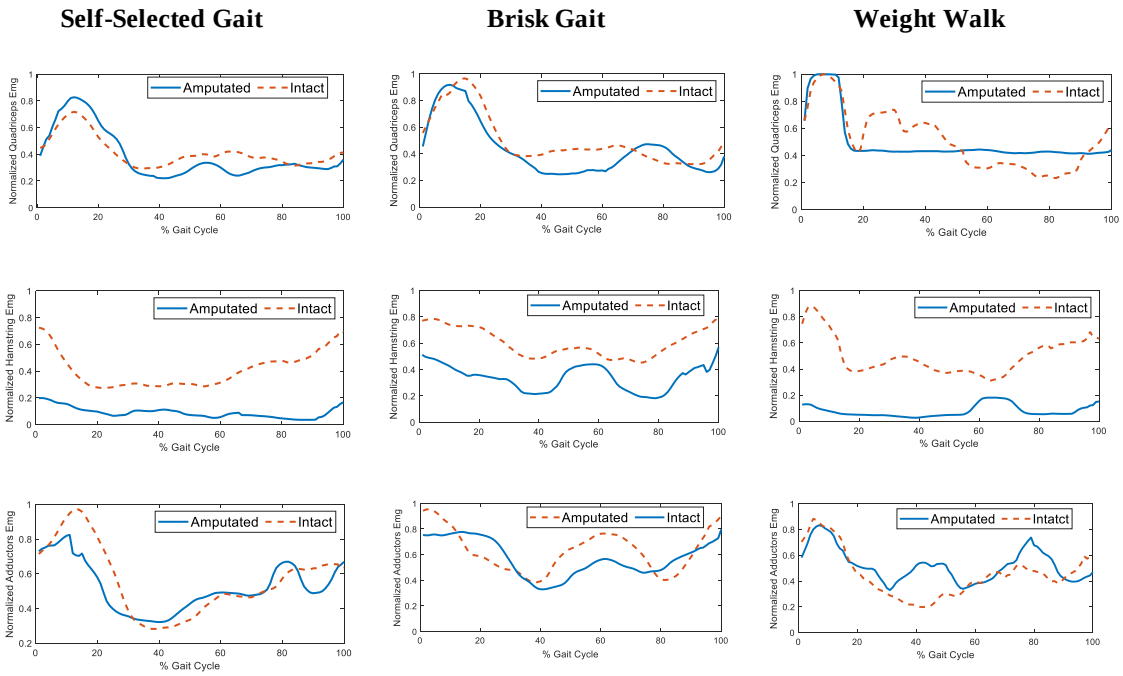

Figure 3.3: Normalized EMG for quadriceps, hamstring, and adductors for self-selected, forward brisk, weight walk gaits in an OTFA subject.

The muscle activity patterns of residual quadriceps and adductors follow a similar pattern to the intact side during self-selected and brisk gait. However, during weight-

bearing walk, these muscles do not exhibit a similar activity trend to the intact side. Additionally, for different types of gaits, the activity of the residual hamstring muscles appears to be significantly lower than that of the intact side.

For question a, in objective 1 of section 3.2, statistical tests were performed to determine if any significant difference existed between $\overline{E_{RMS_{max}}}$ and $\overline{E_{RMS_{min}}}$. Significant difference in these values would imply significant muscle activity occurring at the specified location. Two sample t-tests (two-tailed, paired, unequal variance, alpha = 0.05) were used to validate the following hypotheses.

H1: $\overline{E_{RMS_{max}}}$ equals $\overline{E_{RMS_{min}}}$ in residual quadriceps for OTFA subjects.

H2: $\overline{E_{RMS_{max}}}$ equals $\overline{E_{RMS_{min}}}$ in residual hamstring for OTFA subjects.

H3: $\overline{E_{RMS_{max}}}$ equals $\overline{E_{RMS_{min}}}$ in residual adductors for OTFA subjects.

In these tests, $p > 0.05$ signifies the acceptance of the NULL hypothesis (H = 0), i.e., $\overline{E_{RMS_{max}}}$ is equal to $\overline{E_{RMS_{min}}}$. This will indicate a lack of significant muscle activity. Conversely, $p \leq 0.05$ indicates that the NULL hypothesis is rejected in favor of the alternate hypothesis (H = 1), i.e., $\overline{E_{RMS_{max}}}$ is not equal to $\overline{E_{RMS_{min}}}$. This implies that the corresponding muscle activity occurs with a confidence interval of 95%.

For question b, in objective 1 of section 3.2, integrated EMG (iEMG) signals were calculated from the amputated and intact sides of an osteomyoplastic amputee to compare their respective levels of muscle activity. The following hypotheses were validated to assess whether the muscle activity post-osteomyoplastic amputation resembles that of the intact side:

H4: The residual quadriceps do not exhibit lower activity compared to the quadriceps of the intact limb.

H5: The residual hamstring does not exhibit lower activity compared to the hamstring of the intact limb.

H6: The residual adductors do not exhibit lower activity compared to the adductors of the intact limb.

In order to test the above hypotheses (H4-H6), one-tailed t-tests were used to verify the null hypothesis (H = 0) and the alternate hypothesis (H = 1) as the samples' relationship is in the single direction of interest. In these tests, $p \leq 0.05$ (H = 1) indicates that the corresponding residual muscle activity is lower than the muscle activity in the intact limb. On the other hand, $p > 0.05$ (H = 0) will indicate that the residual muscle activity is not less than (or similar) to the intact side.

3.4.1 Hypothesis Tests Results (Objective 1):

The results from the hypothesis tests H1-H3 are tabulated in Table 2. For quadriceps, the difference between $\overline{E_{RMS_{max}}}$ and $\overline{E_{RMS_{min}}}$ is larger during self-selected gait (0.39±0.033) and brisk gait (0.58±0.223), in comparison to weight walk (0.22±0.086). During self-selected and brisk gait significant muscle activity occurs in quadriceps, hamstring, and adductors muscle groups as $p \leq 0.05$ (null hypothesis is rejected in favor of alternate hypothesis, H = 1). For weight walk, null hypothesis (H = 0) is accepted for all muscle groups. It indicates that there is little muscle activity in the residual muscles during weight walk.

Table 3.2: $\overline{E_{RMS}}$ for quadriceps (Q), hamstring (H), and adductors (A) in OTFA subjects during selected gait activities.

Muscle Group	Hypothesis No	GAIT TYPE	$\overline{E_{RMS_{min}}}$	$\overline{E_{RMS_{max}}}$	H value	p value
Q	H1	Self-Selected (SG)	0.09±0.006	0.48±0.093	1	0.02
		Brisk (BG)	0.11±0.009	0.69±0.232	1	0.03
		Weight Walk (WW)	0.04±0.0007	0.26±0.087	0	0.16
H	H2	Self-Selected (SG)	0.02±0.0006	0.13±0.009	1	0.04
		Brisk (BG)	0.16±0.120	0.45±0.307	1	0.03
		Weight Walk (WW)	0.03±0.001	0.27±0.094	0	0.14
A	H3	Self-Selected (SG)	0.10±0.005	0.37±0.04	1	0.02
		Brisk (BG)	0.15±0.011	0.55±0.115	1	0.04
		Weight Walk (WW)	0.07±0.004	0.204±0.03	0	0.07

The hypothesis test results of H4-H7 are tabulated in Table 3. For all types of gait, and muscle groups, $p \leq 0.05$. Hence, we reject the null hypotheses in favor of the alternate hypotheses, which means that the muscle activities in the residual quadriceps, hamstring, and adductors are less than that in the intact limb's quadriceps, hamstring, and adductors.

3.5 Objective 2 Hypotheses: Effect on Stance Time for OTFA

To investigate the question a and b of objective 2 in section 3.2, the stance time of an osteomyoplastic transfemoral amputee was investigated in comparison to an able-bodied individual. Following two hypotheses have been tested:

H7: A significant difference exists in the stance times between the right and the left leg of a healthy able-bodied individual.

H8: The stance time on the prosthetic limb is smaller than the stance time on the intact limb.

A two-tailed t-test (paired, unequal variance, alpha = 0.05) was used to evaluate H7. Here, $p > 0.05$ ($H = 0$), indicates that the discrepancy between the mean stance times of the right and left leg is zero. Conversely, $p \leq 0.05$ ($H = 1$) indicates that the difference between the mean stance times of the right and left leg is not zero.

To evaluate H8, a one-tailed t-test was used as the samples' relationship is in the single direction of interest. In this case, $p > 0.05$ ($H = 0$) suggests that the intact side's mean stance time isn't greater than the amputated side's mean stance time. While $p \leq 0.05$ ($H = 1$) indicates the opposite- the intact side's mean stance time exceeds that of the amputated side.

Table 3.3: Integrated EMG (iEMG) for quadriceps (Q), hamstring (H), and adductors (A) in OTFA subjects during selected gait activities.

Muscle Group	Hypothesis no	GAIT TYPE	Amputated side	Intact side	H value	p value
Q	H4	Self-Selected (SG)	37.46±225.79	63.64± 268.15	1	0.002
		Brisk (BG)	43.44±178.32	59.19± 248.675	1	0.002
		Weight Walk (WW)	44.29±521.72	58.60±238.58	1	0.02
H	H5	Self-Selected (SG)	12.39±39.90	43.06± 153.83	1	0.009
		Brisk (BG)	28.95±255.25	62.93±165.63	1	0.006
		Weight Walk (WW)	38.81±293.13	54.97±101.80	1	0.03
A	H6	Self-Selected (SG)	43.06±218.56	65.25± 211.41	1	0.015
		Brisk (BG)	49.81±48.59	64.78±166.69	1	0.004
		Weight Walk (WW)	44.13±157.83	58.14±111.12	1	0.03

3.5.1 Hypothesis Tests Results (Objective 2):

The results from the hypothesis tests H7 and H8 are tabulated in Table 4 and 5. For H7, since $p > 0.05$ ($H = 0$), we fail to reject the null hypothesis in favor of the alternate hypothesis indicating there is no significant difference between the stance times of both limbs of an able-bodied individual. For self-selected gait (SG), brisk gait (BG), and weight walk (WW) the mean differences between both legs' stance times for an able-bodied individual are 0.019±0.002, 0.0329, and 0.0133 seconds respectively.

The test results of H8 show that for the OTFA subjects in self-selected gait (SG) and weight walk (WW) the stance time for the intact side is greater than the stance time of the amputated side ($p \leq 0.05$, $H = 1$). This indicates that the OTFA subjects hold more support from their intact side than the amputated side during self-selected gait (SG) and weight walk (WW). For SG, and WW the mean differences between both legs' stance times for OTFA subjects are 0.1889±0.061, and 0.3765±0.0091 seconds respectively. For brisk walk, the difference between intact and amputated sides stance period is not significant ($p > 0.05$, $H = 0$). In this case, the mean difference is 0.0848±0.006 seconds.

Table 3.4: Mean stance time (seconds) in able bodied individuals (ABI) during gait activities.

Subject	Hypothesis no	GAIT TYPE	Right	Left	H value	p value
ABI	H7	Self-Selected (SG)	0.6934±0.006	0.7124±0.004	0	0.44
		Brisk (BG)	0.6249±0.008	0.5920±0.008	0	0.24
		Weight Walk (WW)	0.7445±0.013	0.7312±0.013	0	0.64

Table 3.5: Mean stance time (seconds) in osteomyoplastic transfemoral amputation (OTFA) subjects during gait activities.

Subject	Hypothesis no	GAIT TYPE	Amputated	Intact	H value	p value
OTFA	H8	Self-Selected (SG)	0.7359±0.070	0.9248±0.131	1	0.03
		Brisk (BG)	0.6607±0.014	0.7455±0.008	0	0.09
		Weight Walk (WW)	0.6515±0.031	1.028±0.0219	1	0.01

3.6 Objective 3: Determination of Weight Loading on the Prosthetic Socket of an OTFA

As discussed in section 3.3 Flexforce A201 sensors were placed in the prosthetic socket to measure the contact force at the end of the residual limb. Data was collected at a rate of 500 Hz using a tablet computer in a backpack. The signals were processed, filtered, and normalized to 100% of the gait cycle. Stance and swing phases were identified, and peak and mean pressures during stance were calculated. Figure 3.4 shows the average pressures during different gait activities. It shows that different gait activities result in varying pressure distributions at the end of the residual limb.

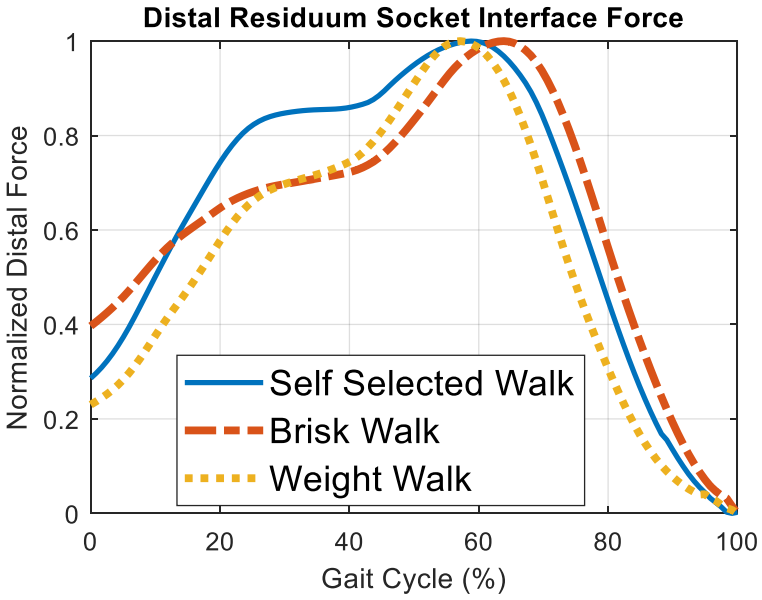

Figure 3.4: Normalized distal residuum socket interface force at self-selected pace, brisk pace, and weight walk.

3.7 Objective 4 Hypotheses: Effect of OTFA on The Intact Side

The impact of amputation on the stance of the intact limb is addressed by measuring the step time (duration from heel strike to heel strike) and stance time (duration when the entire foot is in contact with the ground) of the subjects and determining the ratio of the stance to step time for both legs (Table 3.6). The following hypothesis is used to determine the effect of amputation on the intact limb:

H-0: The mean stance time to step time ratio of the intact limb for amputees is equal to that of able-bodied individuals.

H-A: The mean stance time to step time ratio of the intact limb for amputees is not equal to that of able-bodied individuals.

Table 3.6: Ratio of stance time to step time during normal gait of an individual. (TFA= Transfemoral Amputation, ABI = ABLE Bodied Individual).

S. No	TFA subject's intact side	S. No	ABI subject's corresponding side
S6	0.7032	S1	0.6532
S7	0.7575	S2	0.6035
S8	0.7061	S3	0.6250
S9	0.6891	S4	0.6568
S10	0.8098	S5	0.6589

3.7.1 Hypothesis Tests Results (Objective 4):

Two sample t-tests (two-tailed, paired, unequal variance, alpha = 0.05) were used to validate the hypothesis. The results of the hypothesis test are presented in Table 3.7. Since, P value is less than 0.05 (alpha), we reject the null hypothesis (H-0) in favor of the alternate hypothesis (H-A), that is, the 'ratio of mean stance time to step time' of the intact limb for amputated individual is not equal to the 'ratio of mean stance time to step time' of an intact

limb of an able-bodied individual. This indicates that the amputation also affects the intact limb's gait of a TFA.

Table 3.7: Hypothesis test results (TFA= Transfemoral Amputee, ABI = Able Bodied Individual).

Subject	Mean		H Val.	P Val.
TFA and ABI	TFA subject's intact side: 0.73 ± 0.002	Intact subject's similar side: 0.64 ± 0.005	1	0.005

3.8 Discussion

This research study investigated the impact of OTFA on muscle activity and stance times during three different gaits commonly encountered during daily activity. The study revealed noticeable muscle activity in the residual quadriceps, hamstring, and adductors muscles during self-selected and brisk pace walking. However, muscle activity was less prominent during weight-bearing gait. During the self-selected and brisk gaits, the residual muscle activity pattern follows a similar trend to the intact side. However, the regained muscle function post-amputation remained lower compared to the unaffected side.

Analysis of stance time highlighted gait asymmetry in amputees. Unlike in able-bodied individuals where stance time remains consistent across different gaits (less than 5% difference between both legs), amputees exhibited significant difference in stance times between intact and amputated limb. During normal walking (self-selected and weight walk), the stance time on the prosthetic side was shorter (20%, and 36% shorter) compared

to the intact side, indicating a greater reliance on the unaffected side. This implies noticeable gait asymmetry for an individual with OTFA. In brisk pace, where stance time on the intact side is also reduced, there's no discernible significant difference between the amputated and intact sides (10% shorter than the intact side). This implies that gait asymmetry is less noticeable during brisk pace.

Weight loading profile shows that during differ gait loading profiles differs. Another finding of this study is the effect of amputation on the intact side. It shows that after amputation the stance time ratio on the intact side of an amputee increases compared to an able-bodied individual around 14%.

Comparing the gait of 5 intact individuals to gait of 5 individuals who have undergone through TFA we observed that:

- In able bodied individuals, the muscle activity in both the right and left limbs is similar. On the other hand, there is a significant difference in muscle activity between intact and amputated side of individuals with transfemoral amputation (TFA).
- In individuals with transfemoral amputation, the weight distribution on the prosthetic limb is inconsistent during various gait activities. Over an extended period, these irregular and abnormal loading patterns can have adverse effects on the health of the residual muscles [20].
- Transfemoral amputation not only affects the amputated side but also impacts the intact side. This can lead to gait asymmetry and long-term health consequences.

3.8.1 Special Case

A transfemoral amputee exhibited a Trendelenburg gait due to a mushroom-shaped bone in the distal posterior region, hindering pressure distribution and impeding timely muscle activation for potential contractions.

3.8.2 Limitation of the Study

This study was conducted only with healthy male patients for both intact and amputated subjects. Also, the patients age ranges were around 20-40 years. A larger set of subjects with a broad variances in terms of gender and age should make the study more convincing.

3.9 Conclusions

The muscle activity during laoding response, and gait asymmetry in osteomyoplastic transfemoral amputees during different activities were investigated in this chapter. Results showed consistent muscle contraction for OTFA in self-selected and brisk gait. Gait analysis revealed asymmetry due to longer support on the intact side during normal and weight walk but less asymmetry during brisk walk. Loading responses for OTFA seem to have variations during different types of gait. These findings hold significance in the development of prosthetic legs, assisting amputees in their everyday activities and contributing to long-term health benefits.

Chapter 4 Framework for Modeling and Control of a Prosthetic Leg to Reduce Gait Asymmetry

The first step in the design of a prosthetic control system is to determine a framework for knee-ankle joint. A framework centered around modeling and simulating prosthetic knee-ankle joint dynamics can significantly enhance the study of prosthetic effectiveness during various aspects of gait, such as kinematic behaviors, without subjecting human participants to potential injury risks from prosthetic malfunctions during testing. This chapter will detail the framework for describing the dynamics of the prosthetic knee-ankle joint during gait and implementing control algorithms for knee-ankle joint functionality.

Initially, the dynamics of the prosthetic knee-ankle joint will be elucidated using a link-segment representation. This representation will encompass the interactions between the prosthetic joint and the biological hip joint of the residual leg, alongside considerations for foot-ground interaction and the influence of upper body movements. The aim of this framework is to accurately the complex dynamics involved in prosthetic knee-ankle joint interactions with sufficient accuracy for control design. Differences between the stance times of the legs cause gait asymmetry. A mathematical relation of foot position to knee-ankle joint dynamics will be developed to study the asymmetry in terms of stance time.

Subsequently, the control problem for the prosthetic knee-ankle joint will be formulated as a tracking control problem. This entails developing algorithms that enable the prosthetic joint to accurately track desired trajectories during various gait activities. Additionally, the

chapter will delve into the necessary conditions for implementing these control algorithms effectively, ensuring optimal performance and stability.

By presenting this comprehensive framework, researchers and practitioners can gain valuable insights into the dynamics and control of prosthetic knee-ankle joints, facilitating advancements in prosthetic technology and enhancing the overall quality of life for individuals with limb loss.

4.1 Gait Requirement for Transfemoral Prosthesis[2]

Gait is defined by the movement pattern of the limb while walking. A complete gait cycle while walking can be divided into stance and swing phase [59]. Postural balance of a person during gait depends on the position of the foot and smooth transition of body weight from one leg to another. During the initial portion of the stance, the weight of the body is supported by both the limbs (dual support). As the gait progresses, the entire weight is transferred to the prosthetic limb while the contralateral limb prepares to enter its swing phase. While walking, impaired coordination between joints increases the risk of fall by affecting the motor control of an individual [60]. The nominal displacement profiles for the knee and ankle joints in a healthy individual during normal gait is shown in Figure 4.1. It is desirable for the prosthetic limb to track similar displacement profile in order to achieve near normal gait. Similar to the technique followed in [61], we can calculate the joint angles of lower limb as shown in Figure 4.2. Assuming that the user is walking with upright posture ($\theta_{\text{trunk}} = 90\circ$) and the joints follow the nominal displacement profiles

[2] This chapter has been adapted from: 'An Intelligent Control Approach for Reduction of Gait Asymmetry in Transfemoral Amputees', and 'Neuro-Dynamic Control of an Above Knee Prosthetic Leg' manuscripts by Zunaed Kibria, and Sesh Commuri.

mentioned in Figure 4.1, we can calculate the ideal foot position relative to the ground in a gait (Figure 4.3). The foot makes a positive angle with the ground at 'Heel Strike'. During the transition from 'Foot Flat' to 'Mid-Stance', i.e., from 10% – 25% of the stance phase, the foot is in horizontal position and makes zero degrees with respect to the ground. After 'Heel Off', the foot makes a negative angle with respect to ground and reaches a maximum negative value at 'Toe Off'. The swing phase ensues after 'Toe Off' and the cycle repeats on 'Heel Strike'.

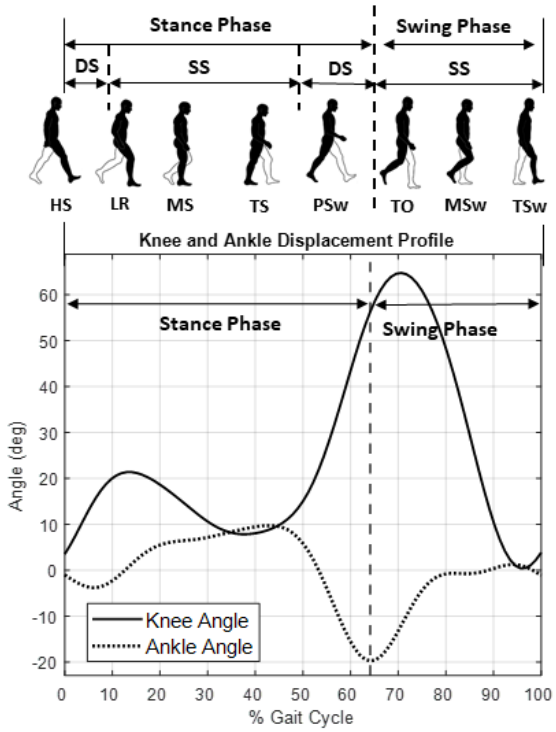

Figure 4.1: Nominal gait profiles for knee, and ankle joints. HS - Heel strike, LR- Loading response, MS= Mid stance, HO – Heel off, PSw- Pre swing, TO - Toe Off, MSw – Mid Swing, TS- Terminal Swing . DS= Dual Support, SS = Single Support.

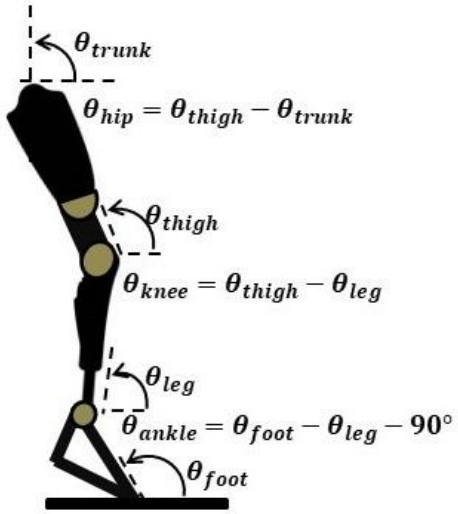

Figure 4.2: Joint angles in the lower limb [62].

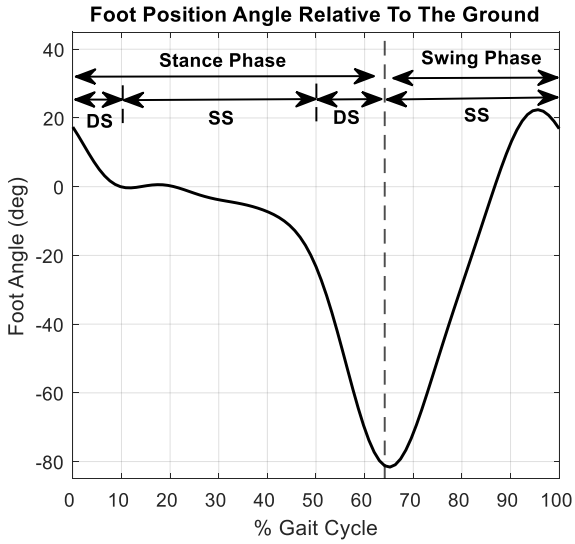

Figure 4.3: Foot position during a gait cycle. DS = Dual support, SS= Single support.

4.2 Gait Modeling and Control of Prosthetic Knee-Ankle Joints

Combining mathematical models with experimental data provides an effective means to explore both normal and pathological gaits. As illustrated in Figure 4.4, a control-oriented

approach is utilized to generate precise control signals, guiding model dynamics along desired trajectories derived from human gait analysis. This approach facilitates the analytical evaluation of various methods for generating joint torques, with potential performance enhancements achieved through feedback adjustments. Similarly, simulation methods that integrate mathematical gait models with experimental data allow for the study of prosthetic effects on kinematic behaviors and other gait aspects, without risking injury due to prosthetic malfunctions during human subject testing. Such frameworks facilitate rapid evaluation of prosthetic device performance under different operating conditions, thereby enhancing understanding of prosthetic leg systems. Additionally, leveraging approaches from robotics systems can benefit the modeling and control of prosthetic devices, as they share common characteristics. These modeling and control approaches not only offer valuable insights into the contributions of muscles and prostheses to the walking mechanisms of individuals with above-knee amputations but also support the development and functional evaluation of future prosthetic devices. However, achieving precise control of prosthetic knee-ankle joints to mimic healthy knee-ankle movement presents several challenges:

a. The optimal knee-ankle displacement profile varies due to factors like individual gait characteristics (e.g., stance time, swing time, step length, and stride length), walking speed, terrain incline, and activity type (e.g., level ground walking, stair climbing/descending). These dynamic factors make it difficult to determine the ideal displacement profile as gait and terrain conditions change, and user intentions are unpredictable.

b. During walking, the movement of the prosthetic foot is influenced by ground reaction forces (GRF) resulting from interactions with the terrain. GRF, essential for supporting body weight, stability, and propulsion, generates a reaction torque at the joint that needs precise compensation for accurate tracking. However, traditional methods for calculating GRF, such as motion tracking systems and force plates, are impractical for prosthetic control during daily activites.

c. The dynamics of the prosthetic foot are influenced by nonlinear coupling effects between the prosthetic knee-ankle joint and the biological hip joints of individuals with above-knee amputations. These interactions are dependent on anthropometric measurements and vary with gait. Neglecting them results in larger tracking errors. Larger tracking error in knee-ankle joints affect the foot position during gait cycle which creates asymmetry in gait.

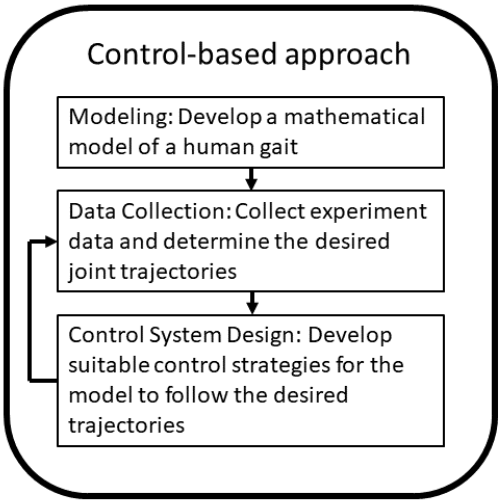

Figure 4.4: Control based approach to the modelling and control of human gait [63].

To tackle these challenges, a framework for modeling and controlling prosthetic knee-ankle joints will be developed-

a. Develop a model that represents the kinematic relationships of the prosthetic leg in the sagittal plane. This model uses link-segment representation and integrates the biological hip joint controlled by the residual leg and the prosthetic knee-ankle joint controlled by an external actuator.
b. Deriving the dynamics of the prosthetic knee-ankle joint from the full gait model, considering knee and ankle dynamics and the influence from other joints. This model will address disturbance torque from the Head-Arm-Trunk and the effect of ground reaction torque.
c. Defining the control objective for the prosthetic knee-ankle joint as the tracking control problem of the desired knee and ankle joint trajectories.
d. Utilizing gait data from amputees to identify gait type and events, enabling the generation of a desired knee-ankle joint displacement profile for developing control algorithms.
e. Estimating gait-based ground reaction torque, compensating for actual ground reaction using an empirical viscoelastic contact model describing foot-ground interaction.
f. Discussing boundary conditions for implementing control algorithms, including bounds on knee-ankle trajectory, ground reaction torque, and disturbance torques.
g. Describing the error dynamic representation of the prosthetic knee-ankle joint to illustrate the relationship between control torque and knee and ankle joints tracking errors.

h. Developing a cost function to assess gait asymmetry by correlating foot movement with tracking errors in knee and ankle joints, aimed at evaluating the efficacy of the control algorithm in minimizing gait asymmetry.

In subsequent chapters, the implementation of machine learning and reinforemenct learning based intelligent control approaches for prosthetic knee-ankle joint control strategies will be elaborated upon.

4.3 Framework for Modeling Prosthetic Knee-Ankle Joint During Gait

In this section, the leg on the amputated side of a person with unilateral above-knee amputation is modeled by a link-segment diagram in the sagittal plane where most of the knee-ankle joint movements occur during gait. This representation includes a biological hip joint, and a prosthetic knee-ankle joint on the prosthetic foot. Euler-Lagrange approach is used to derive the dynamics of this representation. By assuming the total human control of the biological joints, this section then concentrates on dynamics and control of the knee-ankle joint.

Figure 4.5 represents the link-segment diagram of the leg on the amputated side of an individual in the sagittal plane. The dynamics of this diagram can be obtained using the Euler-Lagrange approach [62, 64] and presented as follows:

$$M(\theta)\ddot{\theta} + V(\theta,\dot{\theta})\dot{\theta} + G(\theta) + F(\dot{\theta}) + \tau_d = \tau + \tau_G \tag{4.1}$$

where, $M(\theta)$denotes the inertia matrix of the coupled dynamics representing the knee-ankle system. $V(\theta,\dot{\theta})$denotes for the coriolis/ centripetal matrix. $G(\theta)$ is a vector that

represents the effect of gravity. The frictional terms are represented by $F(\dot{\theta})$. τ_d represents the disturbance torque. On the right side of equation (1), τ represents the torque input to each joint and τ_G represents the torque experienced at each joint due to the ground reaction force. θ, $\dot{\theta}$, and $\ddot{\theta}$ represent joint angles, angular velocities, and angular acceleration.

Assumptions: In the knee ankle joint dynamics presented at (4.1):

- $M(\theta)$ is symmetric, positive definite, and bounded.
- The coriolis/ centripetal matrix $V(\theta, \dot{\theta})$ is bounded. The coriolis/ centripetal matrix can be always selected so that the matrix $\mathrm{S}(\theta, \dot{\theta}) \equiv \dot{M}(\theta) - 2V(\theta, \dot{\theta})$, is skew symmetric.
- Gravity vector $G(\theta)$ is bounded as this is related to weight. $\|G(\theta)\| \leq g_B$
- The disturbance vector τ_d and gound reaction torque τ_g is bounded as these are related to humain gait [24]. $\|\tau_d\| \leq \tau_{dB}$, and $\|\tau_g\| \leq \tau_{gB}$,

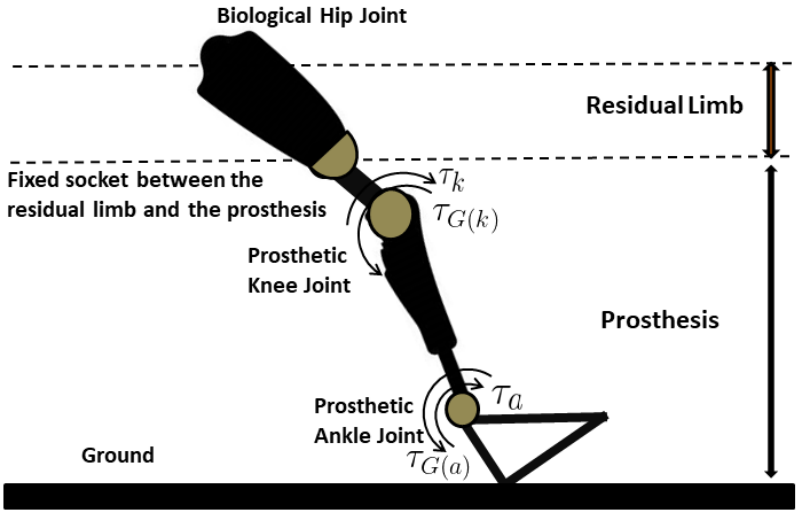

Figure 4.5: Link-segment diagram of the residual limb and prosthetic foot.

4.4 Framework for Control of Prosthetic Knee-Ankle Joint

Commonly used approaches in control of prosthetic keg treat the unknown dynamics in as disturbances and ignore them, thereby degrading the performance and efficiency of the device. These devices are based on linearized dynamics and use proportional-derivative control with fixed control parameters. While these controllers guarantee local stability, their performance might deteriorate quickly in the presence of unmodeled system dynamics and measurement noises. The use of these systems will require prior validation on a large number of subjects under different gait and terrain conditions.

In this framework, the aim is to control the prosthetic leg to mimic natural knee and ankle movements during gait. This involves measuring the effectiveness of control by comparing actual joint positions with desired trajectories, specifically tailored for different types of gait recognized from continuous gait data. Control torque is computed using

various algorithms to adjust the movement of the prosthetic ankle joint accordingly. The goals for the control system of the prosthetic knee-ankle joint are listed below:

- Recognize the type of gait and detect the gait events in real time using actual gait data measured from the users.
- Determine an knee-ankle joint displacement profile corresponding to the selected gait of users.
- Compensate the effect of ground reaction τ_G.
- Implement a control algorithm to generate a control torque τ that provides guaranteed tracking performance.

Detailed discussions on the control framework and problem formulation follow in the subsequent section.

4.5 Recognition of gait and detection of gait events

Identification of walking patterns and identification of key moments in walking can be achieved through the analysis of real-time data collected during walking, such as the forces exerted on the prosthetic socket interface by the residual limb of individuals with below-knee amputation. Utilizing ultra-thin FlexiForce® sensors and a dedicated gait monitoring device, these forces can be accurately measured and monitored even during daily activities outside of controlled laboratory environments.

By integrating these sensors within the socket, continuous and non-intrusive force measurements can be obtained, providing insights into the dynamics of walking. These measurements not only reflect the different types of walking (e.g., normal pace, brisk walking, stair ascent/descent, ramp walking) but also enable the detection of specific

walking parameters such as heel strike, mid-stance, toe-off, and stance time for each step taken.

The comparison between these interface forces and the events recorded by foot switches further validates the relationship between the forces exerted and the specific phases of walking. The characteristic double-peak profile observed in these force profiles corroborates the similarities in weight distribution between the prosthetic and intact sides of individuals with unilateral below-knee amputation, resembling patterns observed in individuals without limb amputations (see Figure 4.6).

Similar methodologies applied in previous studies [65], particularly focusing on features extracted from the forces exerted at the distal end-bearing locations within prosthetic sockets of subjects with transfemoral osteomyoplastic amputations, have shown promise in distinguishing between different walking speeds.

Upon recognition of the type of walking and detection of specific walking events, the control system generates updated references for kinematic parameters and approximations for ground reaction forces tailored to the identified gait pattern. These references are activated at key moments such as heel strike, enabling the proposed control approach to derive suitable torque commands specific to the recognized walking pattern.

In traditional control, the tracking error is computed as the error between the ideal and actual displacement of the joint. In the case of prosthetic knee-ankle joint control, the ideal joint profiles are not available due to unknown users' intent and changes in walking terrain. Therefore, as the first step, approximated knee and ankle joint displacement profiles are generated based on the gait detected in real time.

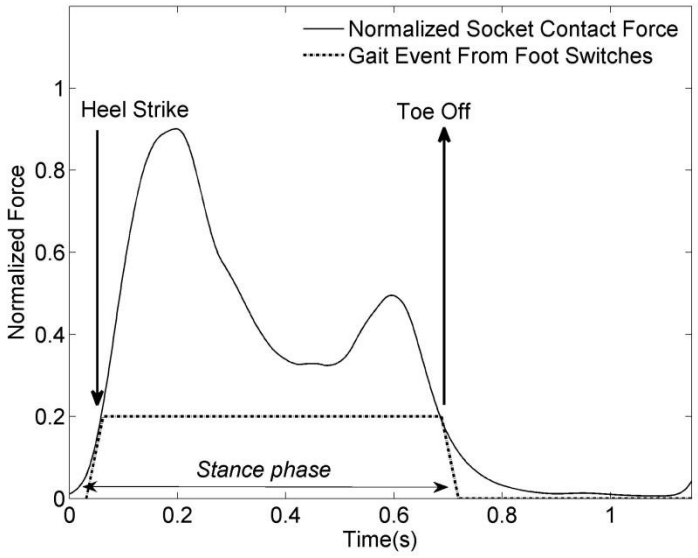

Figure 4.6: Normalized socket contact force and gait events from foot switches [24].

4.6 Parameterization of The Gait Profiles and Ground Reaction Torque

In real life, it is not possible to specify the desired joint displacement profile prior to the individual starting to walk. To circumvent this problem, a nominal stance period is selected for the first step. The actual stance time observed during the first step is then used in the subsequent steps. Nominal displacement profiles collected in the laboratory are parameterized by the stance duration and used to create displacement profiles for knee and ankle joints [61]. These displacement profiles are generated according to (4.2) where the subscript 'i' refers to either knee or ankle joint:

$$\theta^{g}_{r(i)}(t) = a^{g0}_{(i)} + \sum_{k_g=1}^{5}\{a^{g}_{(i)}\cos(k_g\omega^{g}_{(i)}t) + b^{g}_{(i)}\sin(k_g\omega^{g}_{(i)}t)\} \quad (4.2)$$

Here, displacement profile time instance is represented by 't'. We can obtain the parameters $a^{g0}_{(i)}, a^{g}_{(i)}, b^{g}_{(i)}, \omega^{g}_{(i)}$ through the synthesis of the Fourier series. As the hip is under biological control, gait based desired trajectory for 'knee' and 'ankle' can be generated from hip joint

movement and used as kinematic reference as following:

$$\underline{\theta}^{g}_{r(i)}=\left[\theta^{g}_{r(i)} \quad \dot{\theta}^{g}_{r(i)} \quad \ddot{\theta}^{g}_{r(i)}\right];$$

$$\theta^{g}_{r(i)} = \left[\theta^{g}_{kr} \quad \theta^{g}_{ar}\right]^{T};$$

$$\ddot{\theta}^{g}_{r(i)} = \left[\ddot{\theta}^{g}_{kr} \quad \ddot{\theta}^{g}_{ar}\right]^{T};$$

(4.3)

The gait-based profiles are labeled with superscript $(\cdot)^{g}$ and are generated by determining the user's intent during the gait cycle. To compute the control input $\tau + \tau_{G}$, the ideal kinematic profiles of knee-ankle joints $\underline{\theta}_{r(i)} = \left[\theta^{T}_{r(i)} \quad \dot{\theta}^{T}_{r(i)} \quad \ddot{\theta}^{T}_{r(i)}\right]^{T}$ are not available.

The differences between the ideal kinematic references and the gait-based references are defined as:

$$\underline{\tilde{\theta}}^{g}_{r(i)}= \left[\tilde{\theta}^{T}_{r(i)} \quad \dot{\tilde{\theta}}^{T}_{r(i)} \quad \ddot{\tilde{\theta}}^{T}_{r(i)}\right]^{T};$$

$$\tilde{\theta}_{r(i)}=\theta_{r(i)}-\theta^{g}_{r(i)};$$

$$\dot{\tilde{\theta}}_{r(i)}=\dot{\theta}_{r(i)}-\dot{\theta}^{g}_{r(i)};$$

$$\ddot{\tilde{\theta}}_{r(i)}=\ddot{\theta}_{r(i)}-\ddot{\theta}^{g}_{r(i)};$$

(4.4)

In practice, accurate evaluation of ground reaction torque τ_{G} is not feasible. Therefore, gait-based ground reaction torques τ^{g}_{G} acting on knee and ankle joints are estimated from known empirical models.

The estimation errors between estimated GRT τ^{g}_{G} and actual $\tau_{G(i)}$ at the knee or ankle joints are defined as:

$$\tilde{\tau}_{G(i)} = \tau_{G(i)}-\tau^{g}_{G(i)} \; ;$$

(4.5)

The actual ground reaction torque $\tau_{G(i)}$ at knee or ankle joint can be approximated by following equation [24]:

$$\tau^{g}_{G(i)}(t) = d_{z(i)} F_{x(i)}(t) + d_{x(i)} F_{z(i)}(t)\,; \tag{4.6}$$

in which 't' is the gait time, $F_{z(i)}$ indicates the vertical ground reaction force and $F_{x(i)}$ is the horizontal ground reaction forces acting on the knee or ankle joints. $D_{x(i)}$ means the distances between knee joint or ankle joint to the center of pressure (ground contact point) during gait. The ground reaction forces can be computed from a nonlinear spring-damper system equations mentioned in [66]:

$$\begin{aligned} F_{z(i)} &= \bar{\kappa}(z_P)^e + c_m \dot{z}_p \\ F_{x(i)} &= \mu\, F_z\, sgn(\dot{x}_h) \end{aligned} \tag{4.7}$$

in which, z_P and $\dot{z}_p$ mean foot penetration and penetration rate at the ground contact point. $\bar{\kappa}$, e, c_m, μ, $sgn(\cdot)$, $\dot{x}_h$ denote respectively- spring coefficient, spring exponent, damping coefficient, friction coefficient, signum function, and the horizontal velocity.

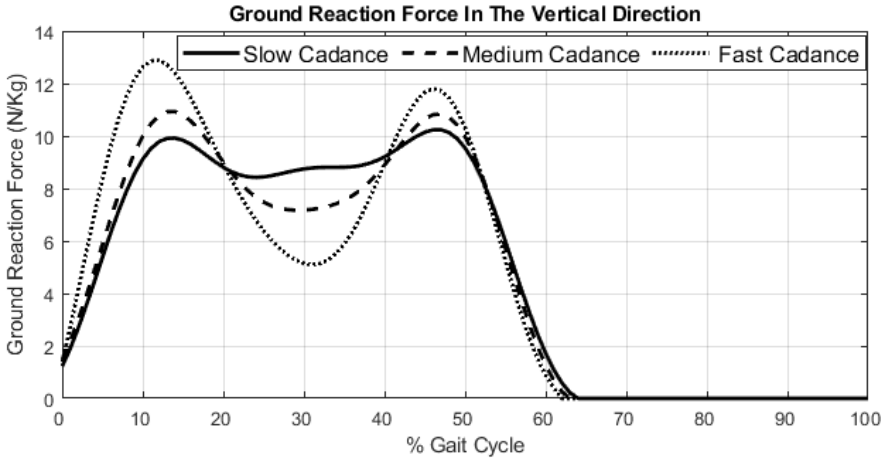

Figure 4.7: Approximated ground reaction force and loading profile from actual foot pressure sensors.

Remark 1. In (4.2), the sine and cosine functions are bounded; it is it is assumed

that the reference kinematic pattern and the gait based kinematic pattern $\theta_{r(i)}^{g}$are also bounded as the residual limb is under active control of the user to follow specific periodic gait profile to reduce the energy consumption during a walk [67]. Hence, we can assume that $\tilde{\theta}_{r(i)}$term is also bounded as it is the difference between two bounded terms.

Remark 2. In (4.7), the ground is assumed to be firm and therefore presents finite penetration of the foot. Therefore, the terms $F_{z(i)}$ and $F_{x(i)}$ terms in equation (4.7) are bounded and gait based $\tau_{G(i)}^{g}$ in (5) is also bounded. Since weight of the individual is known, the actual ground reaction torque $\tau_{\mathrm{G(i)}}$ is also bounded. Therefore, $\tilde{\tau}_{\mathrm{G(i)}} = \tau_{\mathrm{G(i)}} - \tau_{G(i)}^{g}$ is also bounded.

4.7 Gait Profiles Tracking Error and Filtered Tracking Error:

To make the prosthetic system follow a reference trajectory $\theta_{r(i)}^{g}$, at first the tracking error '*e(t)*' and the filtered tracking error '*r(t)*' is defined by:

$$e = \theta_{r(i)}^{g} - \theta;$$

$$r = \dot{e} + \lambda e \tag{4.8}$$

in which, λ is a positive constant, $\theta_{r(i)}^{g} = \begin{bmatrix} \theta_{kr}^{g} & \theta_{ar}^{g} \end{bmatrix}^{T}$; and $\theta = [\theta_k \quad \theta_a]^{T}$;

4.8 Cost Function for Single Support Time

To evaluate the performance of the controller in terms of single support time, a cost function is defined as:

$$\mathrm{J}_{sp}(\mathrm{t}) = \frac{1}{2}\left[e_{ft}(t_{LR})\right]^2 + \frac{1}{2}\left[e_{ft}(t_{TS})\right]^2 \tag{4.9}$$

Here, $e_{ft}(t_{LR})$ and $e_{ft}(t_{TS})$ are the foot angle error of the prosthetic leg from desired foot angle at 'Loading Response' and 'Terminal Stance' phases. Time lapse between these phases of the gait is considered as the single support time t_{SS}.

$$t_{SS} = t_{TS} - t_{LR} \tag{4.10}$$

in which t_{TS} and t_{LR} are the time instances of the prosthetic leg at 'Loading Response' and 'Terminal Stance' phases. If we can minimize e_{ft} at these time instances then it will in turn reduce the single support time error of the prosthetic leg, thereby reducing gait asymmetry. Since the cost function J_{sp} is a function of e_{ft}, so minimizing the cost function will result in reducing gait asymmetry.

Using Figure 4.2 the joint angles can be expressed as:

$$\begin{aligned} \theta_a &= \theta_{ft} - \theta_{lg} - 90°; \\ \theta_k &= \theta_{th} - \theta_{lg}; \\ \theta_h &= \theta_{th} - \theta_{tr}; \end{aligned} \tag{4.11}$$

From "(10)", we can represent the foot angle θ_{ft} as:

$$\begin{aligned} \theta_{ft} &= \theta_a + \theta_h + \theta_{tr} - \theta_k + 90°; \\ \theta_{ft} &= \theta_a + \theta_h - \theta_k + 180°; \ (\theta_{tr} = 90° \text{for upright posture}) \end{aligned} \tag{4.12}$$

At any instant, the angle of the prosthetic foot can be calculated as:

$$\theta_{ft}^{NN} = \theta_a^{NN} + \theta_h - \theta_k^{NN} + 180° \tag{4.13}$$

Subtracting (4.13) from (4.12) we find foot angle error of a NN controlled leg from the reference:

$$e_{ft} = e_a - e_k \tag{4.14}$$

in which, $e_{ft} = \theta_{ft} - \theta_{ft}^{NN}$; $e_a = \theta_a - \theta_a^{NN}$; $e_k = \theta_k - \theta_k^{NN}$;

Inserting, (4.14) to (4.9) the augmented cost function can be written as:

$$J_{sp}(t) = \frac{1}{2}\left[e_a(t_{LR}) - e_k(t_{LR})\right]^2 + \frac{1}{2}\left[e_a(t_{TS}) - e_k(t_{TS})\right]^2 \tag{4.15}$$

4.9 Conclusions

A detailed framework for both modeling and controlling the prosthetic knee-ankle joint was described in this chapter. This framework allows for examining the dynamic interplay between the knee-ankle joints and their interaction with the residual leg joint and the foot-ground interface. The cost function for gait asymmetry is defined based on errors in these joint terms. Controlling these joints will, in turn, help maintain foot position and minimize gait asymmetry. The subsequent chapters will delve into the calculation of knee-ankle torque control using distinct methodologies.

Chapter 5 NEURAL NETWORK-BASED CONTROLLER TOWARDS ACHIEVING NEAR-NATURAL GAIT IN TRANSFEMORAL AMPUTEES.

5.1 Background[3]

Effective control mechanisms are essential for improving prosthetic gait. Many of the available controllers for prosthetic limbs are passive or rely on classical control techniques such as proportional and proportional derivative control. Passive devices can cause loading imbalances and affect walking speed, especially during knee flexion in the stance phase [68]. Active devices based on proportional derivative control do not generate enough propulsion torque during the stance phase due to the unmodeled and nonlinear dynamics of the system [69]. Controllers using data-driven techniques take a long time to tune control parameters and do not focus on gait symmetry [22]. Therefore, alternative control techniques are needed to meet propulsion requirements and to improve gait symmetry.

In this chapter, a neural network-based control strategy is pursued to reduce the asymmetry in gait between the intact and amputated side of an amputee. Gait is primarily divided into two phases: stance and swing. The stance phase is further subdivided into phases including Heel Strike, Loading Response, Mid Stance, Terminal Stance, and Pre-Swing, while the swing phase comprises Toe Off, Mid Swing, and Terminal Swing. During gait, the body weight is supported by a single leg from 'Loading Response' to 'Terminal Stance' phases, and the time difference between these phases is defined as 'single support

[3] This chapter is adapted from 'Reducing gait asymmetry in transfemoral amputees - A neural network based approach' by Zunaed Kibria, Bhanu Prasad Kotamraju, and Sesh Commuri. Journal of Medical Robotics Research, 2024. DOI: https://doi.org/10.1142/S2424905X24400026

time'. When the difference in single support time between the intact and prosthetic side is minimized, it promotes smoother weight transfer between the legs, reduces gait asymmetry, aids amputees in achieving a more natural and balanced gait.

The following approach is adopted to implement a learning controller that can adapt to user requirements and guarantee near natural gait in an individual:

- Develop the dynamical model of the prosthetic leg system to determine the nature of unknown nonlinear functions that influence the dynamics.
- Desired trajectories for the knee and ankle joints are first selected based on the natural displacement profile of these joints in an intact individual and then parameterize in terms of the gait speed.
- Use a visco-elastic model to estimate ground reaction force and reaction torques at the joints, and then compensate for them in the system dynamics.
- A radial basis function (RBF) based neural network is selected to learn the unknown nonlinear parameters in the dynamics. The RBF neural network is preferred due to its efficiency in approximating multivariate functions with faster convergence and lower computational cost [59].
- The cost function reflecting the asymmetry between the gait of the intact and prosthetic side is used to perform Lyapunov analysis. Weight update laws for the neural network are determined so that the unknown/changing dynamics are estimated while ensuring stability of the controlled system and minimizing the cost, i.e., the asymmetry in the gait.

Numerical simulations are used to demonstrate the ability of the control strategy to

accommodate variations in height, weight, gait speed, and ground reaction force. Analysis shows that the time duration of the single support portion of the gait is improved with the proposed control strategy, thereby minimizing the asymmetry in the gait.

5.2 Control Equations

The model for the prosthetic knee-ankle joint and gait asymmetry function J_{sp} has been described in Chapter 4 (equation (4.1), and (4.15)). In order for the prosthetic system to ensure near natural gait cost function J_{sp} needs to be small. From (14) we see that $J_{sp} = fcn(e_k, e_a)$. So, if the controller can reduce the knee and ankle angle error then in tern it will reduce J_{sp} . To make the prosthetic system follow a reference trajectory $\theta^g_{r(i)}$, at first the tracking error *'e(t)'* and the filtered tracking error *'r(t)'* is defined by:

$$e = \theta^g_{r(i)} - \theta;$$

$$r = \dot{e} + \lambda e \tag{5.1}$$

in which, λ is a positive constant, $\theta^g_{r(i)} = \begin{bmatrix}\theta^g_{kr} & \theta^g_{ar}\end{bmatrix}^T$; and $q = [\theta_k \quad \theta_a]^T$; The dynamics of the prosthesis in (4.1) can be expressed with reference to the filtered tracking error as:

$$\mathrm{M}\dot{r} = M\left(\ddot{\theta}^g_{r(i)} - \ddot{\theta} + \lambda\dot{e}\right)$$

$$= -\mathrm{V}r + f + \tau_\mathrm{d} - \tau - \tau_\mathrm{G} \tag{5.2}$$

Where, $f = M\left(\ddot{\theta}^g_{r(i)} + \lambda\dot{e}\right) + V\left(\dot{\theta}^g_{r(i)} + \lambda e\right) + G(\theta) + F(\theta)$.

The term f comprises of the unknown nonlinear terms in the dynamics of the system. In the next sections, we will demonstrate the use of RBF neural network to approximate f and implement a stable controller.

5.3 Neural Network (NN) Based Approximation

The function f in (5.2) is a smooth function of the joint angles and joint velocities and can be bounded on a compact region in $\mathbb{R}^2$. Hence f can be approximated using a RBF network [59].

The output of the RBF network (Figure 5.1) can be expressed as:

$$h_j = exp^{-\frac{\|x-\mu_i\|}{b_j}} ; j = 1,2,3,..k$$

$$f(x) = \underline{W}^T h + \varepsilon \tag{5.3}$$

in which, x is the input of the network, μ_i value represents the center point of the Gaussian function of the neural net k for the i^{th} input, b_j is the width of the Gaussian function for neural network k. Here, $\underline{W}$ represents optimum weight for the NN and ε is a very small value. For an estimated value of $\underline{W}$, i.e. $\widehat{W}$, the output of the NN is expressed as $\widehat{W}^T$h(x). Learning algorithms are designed such that $\widehat{W}$ is updated iteratively to minimize the error between *f(x)* and its estimation $\hat{f}$(x).

$$\hat{f}(x) = \widehat{W}^T h(x) \tag{5.4}$$

Here, $\widetilde{W} = \underline{W} - \widehat{W}$; $\|\underline{W}\|_F \leq W_b$; so, $\dot{\widetilde{W}} = -\dot{\widehat{W}}$;

$$f - \hat{f} = \tilde{f} = \underline{W}^T h + \varepsilon - \widehat{W}^T h = \widetilde{W}^T h + \varepsilon \tag{5.5}$$

From the *f(x)* expression in equation (5.2) the input of the RBF has been selected as:

$x = \left[e_k \;\; \dot{e}_k \;\; e_a \;\; \dot{e}_a \;\; \theta_{kr}^g \;\; \dot{\theta}_{kr}^g \;\; \ddot{\theta}_{kr}^g \;\; \theta_{ar}^g \;\; \dot{\theta}_{ar}^g \;\; \ddot{\theta}_{ar}^g \right]$; here, subscript k= knee, a=ankle, r = reference; superscripts g = gait-based.

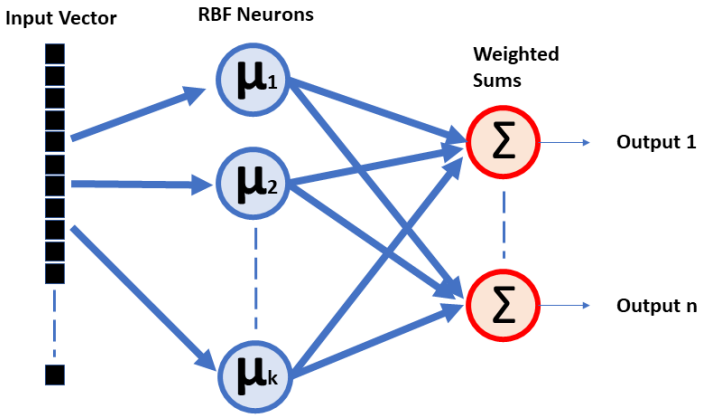

Figure 5.1: Structure of a Radial Basis Function.

The control law for the system described in (5.2) is:

$$\tau = \hat{f}(x) + K_v r - \upsilon - \tau_G^g \tag{5.6}$$

In which, $\hat{f}$ is the estimation of f, $\upsilon = -(\varepsilon_N + b_d)sgn(r)$ is the robust term, and τ_G^g is the gait-based ground reaction torque. The corresponding neural network adaptive law is designed as:

$$\dot{\hat{W}} = Fhr^T - \kappa F\|r\|\hat{W} \tag{5.7}$$

Where, κ, $F = F^T \geq 0$ are design parameters. In (5.7) the third term is the filtering term which gives a better tracking response for non-zero initial condition.

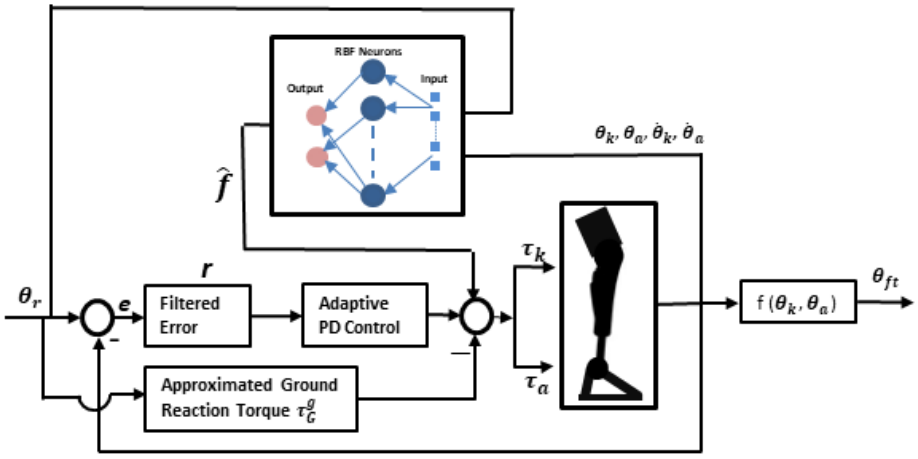

Figure 5.2: Block diagram of the neural network controlled prosthetic leg system.

Theorem VI.I. The prosthetic system given in (5.2) with the control law in (5.6) and the weight update law for the NN in (5.7) ensure that J_{sp} is bounded and the error between the desired and actual support time can be made arbitrarily small. Further, the tracking error *e(t)* is bounded and can be made arbitrarily small.

Proof.

Substituting (5.6) to (5.2) we can find:

$$\begin{aligned} M\dot{r} &= -Vr + f(x) + \tau_d - \left(\hat{f}(x) + K_v r - \upsilon - \tau_G^g\right) - \tau_G; \\ &= -(K_v + V)r + \tilde{f}(x) + \tau_d - (\tau_G - \tau_G^g) + \upsilon \\ &= -(K_v + V)r + \tilde{W}^T h + \varepsilon + \tau_d - \tilde{\tau}_G + \upsilon \end{aligned} \tag{5.8}$$

Where, $\tilde{\tau}_G$ is the difference between actual and gait-based ground reaction torque.

First, the Lyapunov function is defined as:

$$L = \frac{1}{2} r^T M_{ka} r + \frac{1}{2} tr\left(\widetilde{W}^T F^{-1} \widetilde{W}\right) \quad (5.9)$$

Taking derivative of *(5.9)*we can find:

$$\dot{L} = r^T M \dot{r} + \frac{1}{2} r^T \dot{M} r + tr\left(\widetilde{W}^T F^{-1} \dot{\widetilde{W}}\right), \quad (5.10)$$

Inserting (5.4), (5.8) into (5.10), we can find:

$$\dot{\mathrm{L}} = -\mathrm{r}^{\mathrm{T}} K_v r + \frac{1}{2} \mathrm{r}^{\mathrm{T}}\left(\dot{M} - 2V\right)\mathrm{r} + \mathrm{r}^{\mathrm{T}}\left(\widetilde{W}^T h + \tau_{\mathrm{d}} - \tilde{\tau}_G + \upsilon + \varepsilon\right) - \mathrm{tr}\left(\widetilde{\mathrm{W}}^{\mathrm{T}} \mathrm{F}^{-1} \dot{\widetilde{\mathrm{W}}}\right) \quad (5.11)$$

Due to skew symmetric characteristic of the third term of (5.11) $\left(\dot{\mathrm{M}} - 2V\right) = 0$, so we can rewrite the equation, with the help of (5.5) as:

$$\dot{\mathrm{L}} = -\mathrm{r}^{\mathrm{T}} K_v r - \mathrm{tr}\left\{\widetilde{\mathrm{W}}^{\mathrm{T}}\left(\mathrm{F}^{-1}\dot{\widetilde{\mathrm{W}}} - h\mathrm{r}^{\mathrm{T}}\right)\right\} + \mathrm{r}^{\mathrm{T}}(\tau_{\mathrm{d}} - \tilde{\tau}_G + \upsilon + \varepsilon); \quad (5.12)$$

Substituting the value from (5.7) to (5.12)we can find:

$$\dot{\mathrm{L}} = -\mathrm{r}^{\mathrm{T}} K_v r + \kappa \|r\| tr\left\{\widetilde{\mathrm{W}}^{\mathrm{T}}\left(\underline{W} - \widetilde{W}\right)\right\} + \mathrm{r}^{\mathrm{T}}(\tau_{\mathrm{d}} - \tilde{\tau}_G + \upsilon + \varepsilon); \quad (5.13)$$

The fourth term in the equation (5.13) can be written as:

$$\begin{aligned} &\mathrm{r}^{\mathrm{T}}(\tau_{\mathrm{d}} - \tilde{\tau}_G + \upsilon + \varepsilon) \\ &= \mathrm{r}^{\mathrm{T}}(\tau_{\mathrm{d}} - \tilde{\tau}_G + \varepsilon) + \mathrm{r}^{\mathrm{T}}\{-(\varepsilon_N + b_d) sgn(r)\} \\ &= \mathrm{r}^{\mathrm{T}}(\tau_{\mathrm{d}} - \tilde{\tau}_G + \varepsilon) - \|\mathrm{r}\|(\varepsilon_N + b_d) sgn(r) \leq 0 \end{aligned} \quad (5.14)$$

Where, $\varepsilon_N > \varepsilon$ and $b_d > \tau_{\mathrm{d}} - \tilde{\tau}_G$. So, this term is bounded.

Since the fourth term of (5.13) is bounded and $tr\left\{\widetilde{\mathrm{W}}^{\mathrm{T}}\left(\underline{W} - \widetilde{W}\right)\right\} \leq \left\|\widetilde{W}\right\|_F \left(W_B - \left\|\widetilde{W}\right\|_F\right)$

we can write:

$$\dot{L} = -\mathrm{r}^{\mathrm{T}} K_v r + \kappa \|r\| tr\left\{\widetilde{\mathrm{W}}^{\mathrm{T}}\left(\underline{W} - \widetilde{W}\right)\right\} + \mathrm{r}^{\mathrm{T}}(\tau_{\mathrm{d}} - \tilde{\tau}_G + \upsilon + \varepsilon)$$

$$\leq -K_v\|r\|^2 + \kappa\|r\|\left\|\widetilde{W}\right\|_F\left(W_B - \left\|\widetilde{W}\right\|_F\right) + (\varepsilon_N + b_d)\|\mathrm{r}\|$$

$$= -\|\mathrm{r}\|\left\{K_{vmin}\|\mathrm{r}\| + \kappa\left\|\widetilde{W}\right\|_F\left(\left\|\widetilde{W}\right\|_F - W_B\right) - (\varepsilon_N + b_d)\right\} \qquad (5.15)$$

By setting up boundary for $\|\mathrm{r}\|$ and $\left\|\widetilde{W}\right\|_F$ as:

$$\|r\| > \frac{\frac{\kappa}{4}W_b^2 + (\varepsilon_N + b_d)}{K_{vmin}} = \frac{B_1}{K_{vmin}} = B_r$$

$$\left\|\widetilde{W}\right\|_F > \frac{W_b}{2} + \sqrt{\frac{1}{4}W_b^2 + \frac{(\varepsilon_N + b_d)}{\kappa}} = B_w \qquad (5.16)$$

We can observe that in (5.15), $\dot{L}$ is negative because the term inside the braces can be written as:

$$\left\{K_{vmin}\|\mathrm{r}\| + \kappa\left\|\widetilde{W}\right\|_F\left(\left\|\widetilde{W}\right\|_F - W_B\right) - (\varepsilon_N + b_d)\right\}$$

$$= \kappa\left(\left\|\widetilde{W}\right\|_F - \frac{1}{2}W_B\right)^2 - \frac{\kappa}{4}\mathrm{W_b^2} + \mathrm{K_{vmin}}\|\mathrm{r}\| - (\varepsilon_N + b_d)\} \qquad (5.17)$$

The first and third terms on the right side of (5.17) are positive and other terms are negative. The boundary conditions of (5.16) ensure that the derivative of the Lyapunov function (5.15) is negative on the region described in (5.16) and implies system stability. The boundary conditions of (5.16) ensure the filtered tracking error and the error in estimated NN weights converge exponentially to the bounds expressed in (5.16). Now, from (5.1) and (5.16), we can set the bounds for error terms as:

$$\|\mathrm{e}\| < \frac{\|\mathrm{r}\|}{\lambda_{\min}} < \frac{\mathrm{B_1}}{\lambda_{\min}\mathrm{K_{vmin}}} \qquad (5.18)$$

Where, $\lambda_{\min}$ is the minimum design value for λ.

From (4.9) we see that the cost function J_{sp} depends on the difference between e_a and e_k. From (4.9) and (5.18) we can write:

$$\frac{1}{2}(e_a - e_k)^2 < \frac{1}{2}(\|e_a\| + \|e_k\|)^2 < \frac{1}{2}\left(\frac{2B_1}{\lambda_{min} K_{vmin}}\right)^2 \qquad (5.19)$$

Which gives a bound on the cost function J_{sp} in (4.9).

$J_{sp} < \left(\frac{2B_1}{\lambda_{min} K_{vmin}}\right)^2$; Therefore, it can be concluded that the cost function J_{sp} is bounded by design terms λ_{min} and K_{vmin}, and can be minimized by the choice of design values.

5.4 Simulation Result

In this section, three simulation examples are considered to compare the performance of the proposed controller with a standard PD controller ($\tau^{PD} = K_v^{PD}(\lambda^{PD} e + \dot{e}) - \tau_G^g$) which is widely used for this type of systems. The parameters used for the simulations are given in the Appendix. The system parameters for the model were selected as described in [70, 71]. Gain parameters for both PD and NN controllers were chosen to provide stable and acceptable tracking performance. Lowering the gain values causes tracking performance to deteriorate and ultimately results in an unstable system.

5.4.1 Near Natural Gait

In this example, the gait with the prosthetic leg is compared with the gait of an intact individual. The resulting foot position angle with respect to ground in shown in Figure 5.3. It is seen that the NN controller maintains desired foot angle profile whereas a standard PD-controller cannot track the desired foot profile accurately.

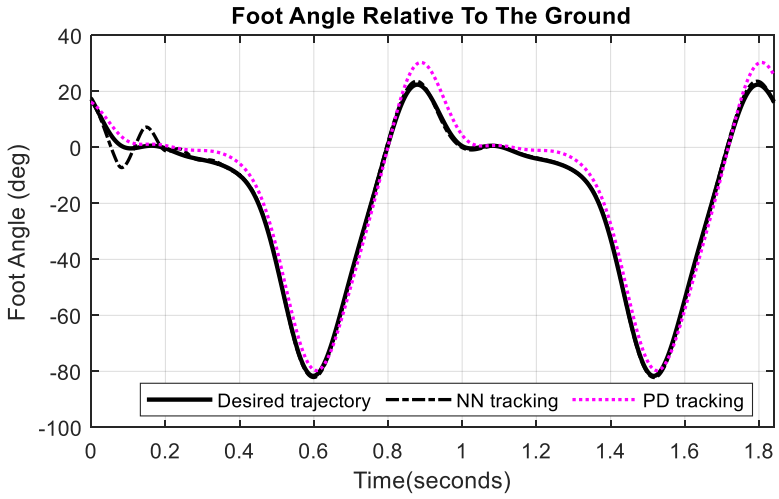

Figure 5.3: Foot profile tracking performance of neural network and PD controller.

In Figure 5.4, we plotted the calculated foot angle error values from desired values with respect to the ground at 'Heel Strike (HS)', 'Loading Response (LR)', 'Mid Stance (MS)', 'Terminal Stance (TS)', and 'Toe-Off (TO)' phases for both the proposed and PD controllers. In all the five cases considered in this paper, the foot position achieved using the PD controller is significantly worse than that achieved by the NN controller leading to gait asymmetry.

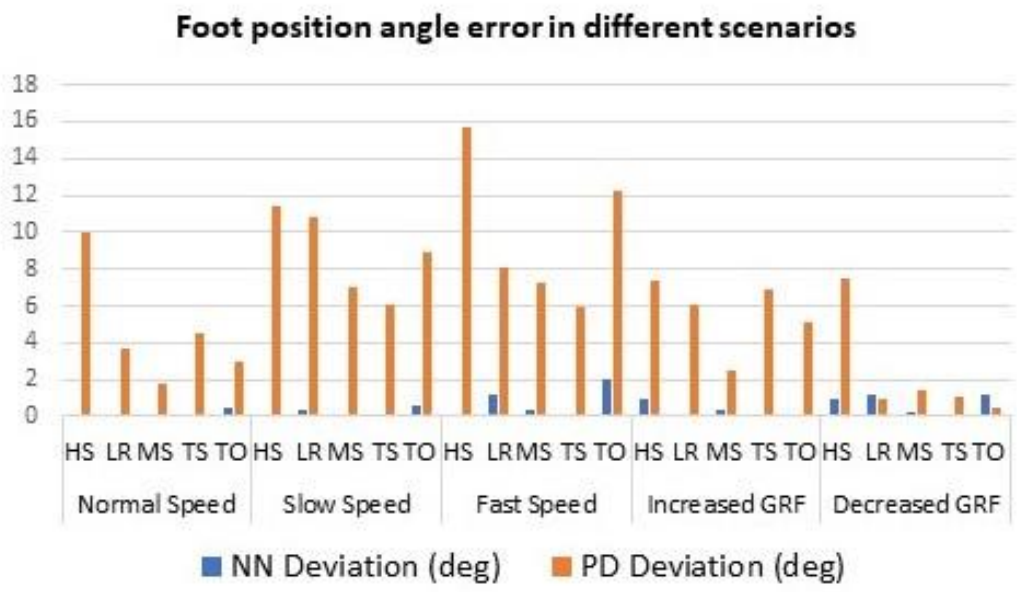

Figure 5.4: Foot position angle error in different scenarios for NN and PD controller in stance phase. HS = Heel Strike, LR = Loading Response, MS = Mid Stance, TS = Terminal Stance, TO = Toe Off.

In Figure 5.5 we plotted the tracking error to observe the effect of robust term in (5.6).

Without the robust term the performance of the NN based controller deteriorates but still it performs better than PD controller.

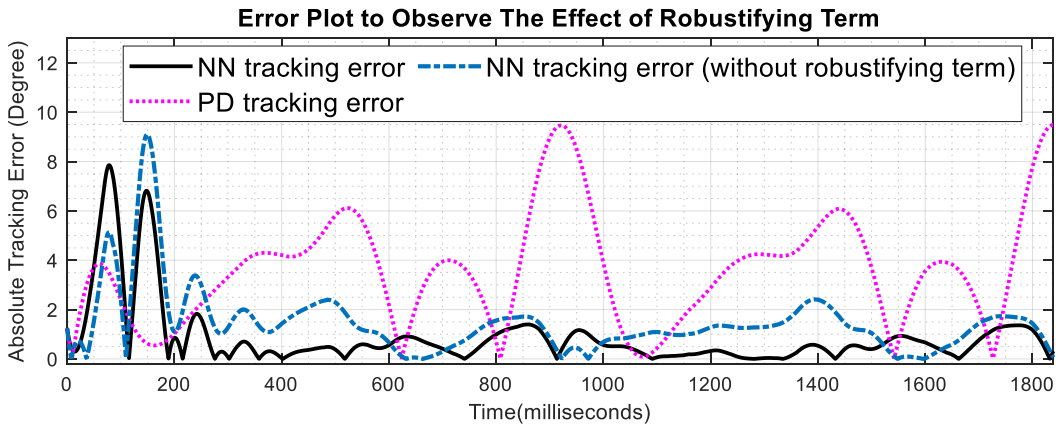

Figure 5.5: Foot profile tracking performance of the controllers to observe the effect of robust term.

5.4.2 Monte-Carlo Simulation to Study Support Time

In the second example, Monte Carlo simulation is performed to study the 'support time' achieved by the proposed controller. Support time is defined by the time difference between the 'Loading Response (LR)' and 'Terminal Stance (TS)' phases of the gait. In this example, 1000 different simulations are conducted with the walking speed, ground reaction force, measurement noise, disturbance torque being randomly selected. The error between the desired support time and the actual support time (TS and LR time error) is shown in Figure 5.6. It is seen that the proposed controller can achieve near-normal gait despite unknown changes in user gait, terrain conditions, or measurement noise (error in LR and TS time is 6.74 and 5.03 milliseconds (standard deviation of 0.13 and 0.29 milliseconds)). On the other hand, the performance of PD controller deteriorates in the presence of variations in desired gait, terrain conditions, and measurement noise (error in LR and TS time is 148.76 and 153.94 milliseconds (standard deviation of 0.97 and 0.58 milliseconds)).

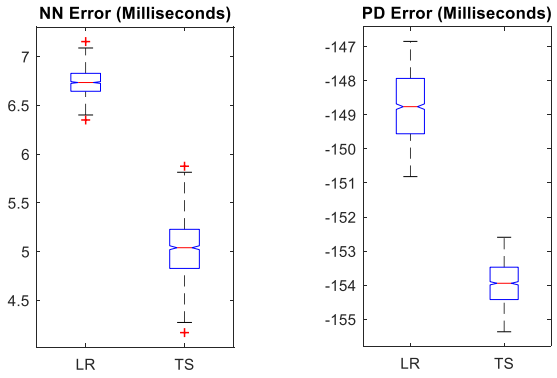

(a) (b)

Figure 5.6: Monte Carlo error for NN (a) and PD (b) at Loading Response (LR), and Terminal Stance (TS) phases.

5.4.3 Tracking Performance

The tracking performance for nominal gait (walking at normal self-selected pace, known ground reaction force, and no disturbance torque) is considered in this example. From Figure 6, it is seen that the NN controller can track the desired knee and ankle displacement profiles with greater accuracy than the PD controller.

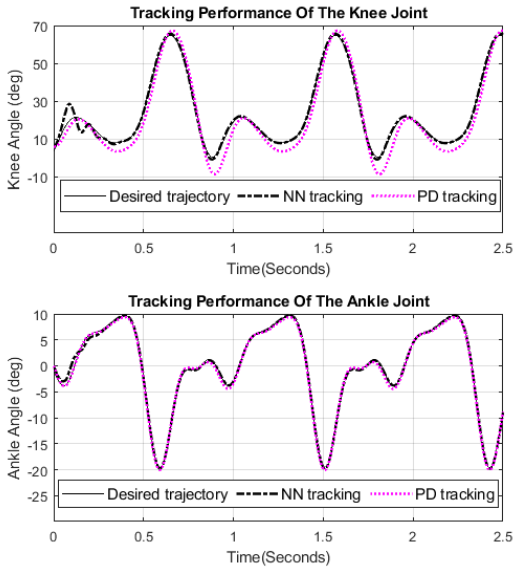

Figure 5.7: Tracking performance of the controllers for knee-ankle joints.

The tracking performance is studied when the conditions on nominal gait are relaxed (±35% ground reaction force, +10% disturbance torque and measurement noise, different speed). Figure 7 shows that the tracking error is lower for the proposed controller compared to the PD controller.

The simulation examples discussed in this section demonstrate that the proposed NN controller can adapt in real time to track desired joint profiles for the prosthetic leg. More importantly, the proposed controller ensures that the prosthetic foot reaches the 'Loading Response' position and maintains stipulated 'single support time' to provide near natural gait for the individual.

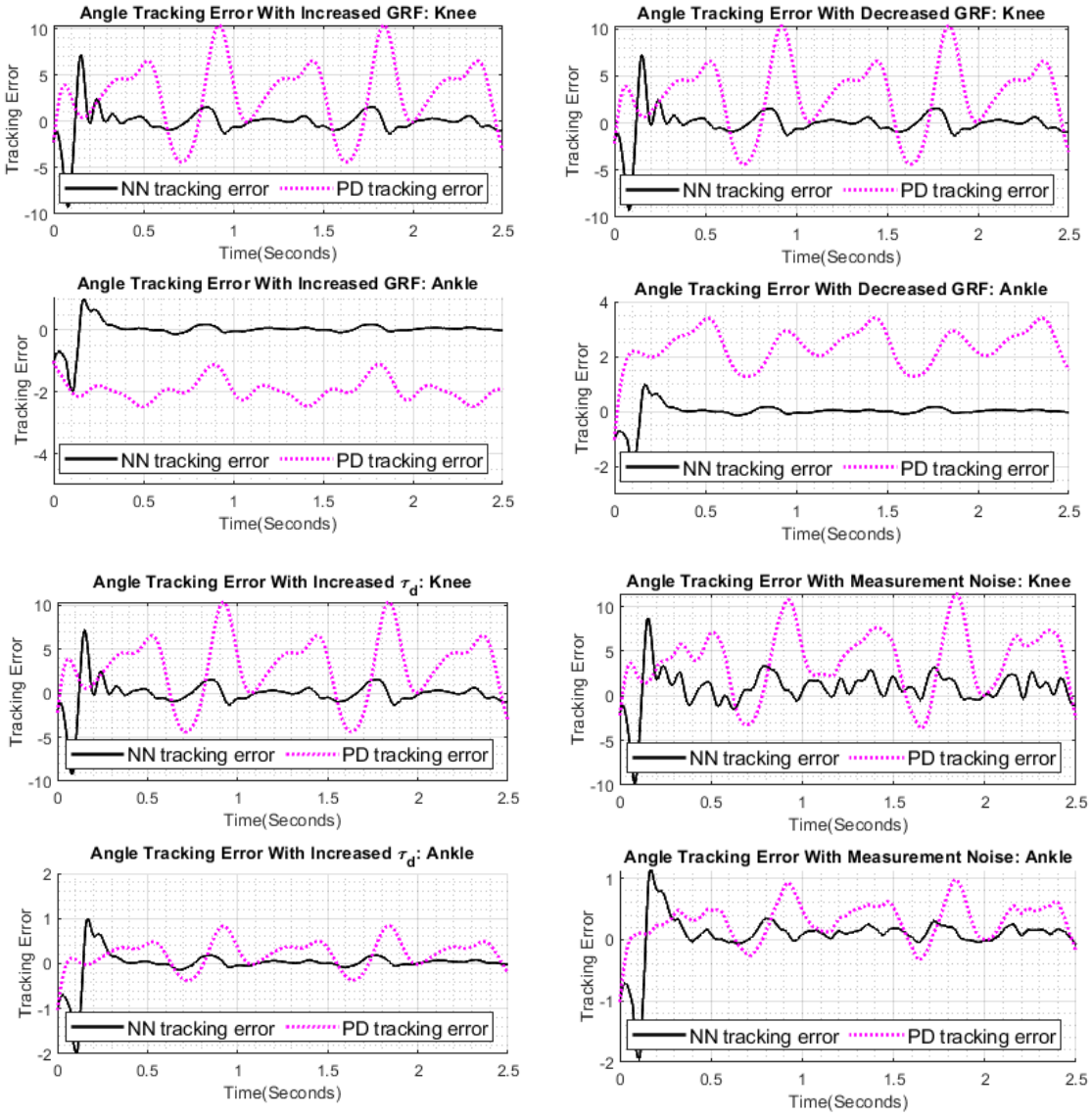

Figure 5.8: Tracking performance of the controllers with variable ground reaction forces, system disturbance, and noise.

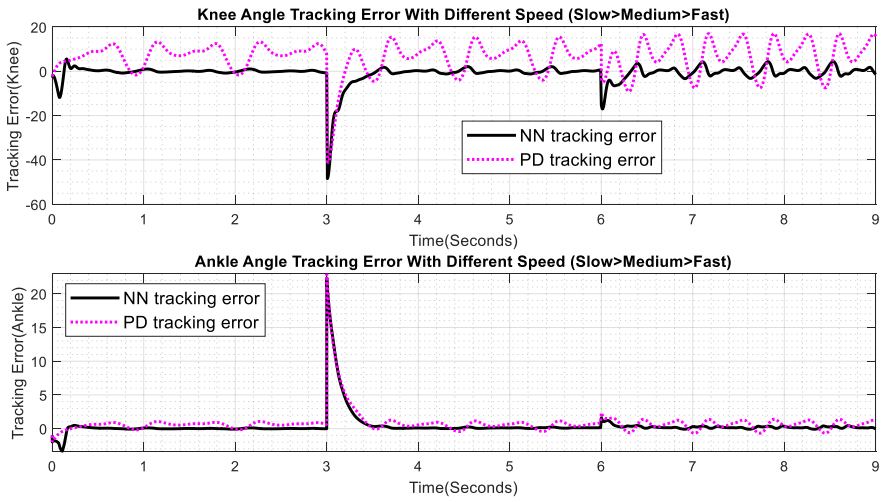

Figure 5.9: Tracking performance of the controllers in difference gait speed.

5.5 Conclusions

In this chapter, a novel control strategy was proposed to reduce the asymmetry in gait between the intact and amputated side of an amputee. Unlike traditional controlling approach, the proposed controlling approach effectively addresses real time challenges like variations in ground reaction force, measurement noise, changes in walking speed etc., that can degrade the performance of the system. The proposed controller can maintain the foot position within 1◦ and support time between 4-7 milliseconds from the corresponding values on the intact side, notably reducing gait asymmetry and achieve natural locomotion. It holds great promise for prosthetics, potentially enhancing amputee mobility, comfort, and overall quality of life. The development of a prosthetic test-bed and the validation of the control strategy discussed in this chapter are subject of ongoinf research.

Chapter 6 NDP BASED CONTROL OF A PROSTHETIC LEG

6.1 Background[4]

Above-knee amputation significantly impacts daily life and long-term mental and physical health of an individual [72]. A well-fitted prosthetic device is necessary to prevent complications like pressure sores and gait asymmetry, and plays a crucial role in rehabilitation [43]. In addition to providing adequate support to the individual during stance, an ideal prosthetic device should facilitate near-natural gait, adapt to user intent, and adjust the joint movements for varying speeds and terrains in real-time.

While the primary function of a prosthetic leg is to provide support during stance, the ability to provide near-natural gait is essential to the long-term health of the individual. Asymmetric gait can cause individuals to expend more metabolic energy [73]. Asymmetric gait can also lead to serious long-term injuries and poor quality of life [74]. Impaired gait in the elderly can lead to dementia and other neurological diseases [75]. Therefore, it is desirable for the prosthetic device to reduce gait asymmetry between the intact and amputated side.

Current passive devices cannot adapt to changing user needs and cause the individual to use excess metabolic energy during locomotion [76-78]. Commercially available powered prosthetic legs are heavy, have limited functionality, and are not suited for prolonged use [79, 80]. Model reference adaptive control-based systems can account

[4] This chapter is adapted from "Neuro-dynamic Control of an above Knee Prosthetic Leg" by Zunaed Kibria and, Sesh Commuri. Accepted in Springer Nature Computer Science, 2024.

for unknown dynamics but their performance is limited to a narrow region of operation due to their use of linearized models [8].

Several companies such as Ossur, Ottobock, SpringActive, BionX Medical Technologies, Freedom Innovations etc., have commercialized active-powered limbs [81]. Though these devices provide good performance in terms of locomotion, they use traditional control techniques based on linear approximations of the system and are unable to compensate for unmodeled dynamics. Further, the control parameters of these devices have to be adjusted to address the requirements of each individual. Several researchers explored the use of neural networks and reinforcement learning to control artificial knee and ankle joints with varying degrees of success [24, 80, 82]. However, these approaches ignore the coupled dynamics between the knee and the ankle thereby limiting the performance of these devices. Further, these approaches do not guarantee "near-natural" gait or reduce the asymmetry between the intact and the prosthetic limb. Therefore, use of these devices could result in potential health complications over time.

Neuro-dynamic programming (NDP) has shown promising results in the control of uncertain complex dynamical systems [83-85]. NDP is based on approximation theory and uses Bellman's optimality principle to improve the control decision at each step to result in a lower long term cost [86]. However, traditional optimal control had limited success in the control of prosthetic leg [87, 88]. Popular deep learning and reinforcement learning based algorithms such as gray wolf optimizer [89], and through rule-based approximation and visualization [90], have been shown to be effective in learning from large data sets.

However, these algorithms are based on offline learning [90] or have slow convergence speeds [89], thus making them unsuitable for real-time control of prosthetic limbs.

In this chapter, a neuro-dynamic control approach for above-knee prosthetic systems is implemented to address gait asymmetry and attain a more natural walking pattern. The controller functions through two networks. First, the Actor Network uses filtered tracking error to compute the instantaneous control needed for precise joint movement along prescribed displacement profiles. Secondly, the Critic Network calculates the "to go" cost, adjusting control actions to minimize long-term expenses, gradually improving the controller's effectiveness after each stance phase during walking. For this approach to be successful, desired knee and ankle displacement profiles are determined using intact-side gait data. The filtered tracking error system generates control torque, enabling the knee and ankle joints to replicate the prescribed trajectories. A neural network learns the system's dynamics, updating Critic Network weights after each stance phase to minimize lookahead costs. Simulation results reveal improved alignment of knee and ankle joints, along with the foot angle with the ground, resembling intact-side profiles, thus enhancing stance and reducing asymmetry. Several monte carlo simulations have been performed to study the perofrmance of the controller over varying gaits. The rfesultsd show that the proposed neuro-dynamic controller performs better than both adaptive neural network (NN) and traditional PD controllers.

6.2 Controller Design

The model of the knee-ankle joint system has been described in (4.1).

To design a controller to track the gait profiles shown in **Error! Reference source not found.**, we first define the tracking error vector 'e' and its derivative 'ė' as follows:

$$e = (\theta_r - \theta)$$

$$\dot{e} = \left(\dot{\theta}_r - \dot{\theta}\right) \tag{6.1}$$

Where, $\theta_{\mathrm{r}} = [\theta_{rk} \quad \theta_{\mathrm{r}a}]^T$; $\dot{\theta}_{\mathrm{r}} = [\dot{\theta}_{\mathrm{r}k} \quad \dot{\theta}_{\mathrm{r}a}]^T$; $\theta_{rk}, \theta_{ra}, \dot{\theta}_{rk}, \dot{\theta}_{ra}$ are desired angular positions and velocities for knee and ankle joints. The dynamics of the system in equation (1) can be represented using the filtered tracking error 'r' as

$$r = \dot{e} + \lambda e \tag{6.2}$$

where, r is a 2x1 dimensional vector and $\lambda > 0$ is a design parameter. Using equation (6.1), we can represent the dynamics of the prosthetic system **Error! Reference source not found.** as

$$M\dot{r} = -Vr + f(x) - \tau \tag{6.3}$$

where, $f(x)$ comprises the nonlinear terms of the system.

$$f(x) = M\left(\ddot{\theta}_r + \lambda\dot{e}\right) + \mathrm{V}\left(\dot{\theta}_r + \lambda e\right) + \mathrm{F} + \mathrm{G} - \tau_G + \tau_d$$

To estimate the nonlinear terms of the system, we propose a neuro-dynamic control structure that will learn the unknown dynamics of the system. This structure generates input τ for knee and ankle joints to ensure a smooth gait and minimize the long-term cost function:

$$\tau = \hat{f}(\mathrm{x}) + K_v r - \upsilon \tag{6.4}$$

where, $\hat{f}(\mathrm{x})$ is the estimation of $f(x)$, K_v is design parameter, r is the filtered tracking error, $\upsilon = -\acute{\upsilon} sgn(r)$ is a robustifying term.

In designing the proposed controller, we've considered the interval from heel strike (HS) to the succeeding heel strike (HS) as a single gait cycle. At each instance within this cycle, we've defined short-term costs for both the knee and ankle joints based on their tracking errors. The short-term cost function of the prosthetic system is represented as a 2x1 dimensional vector S(t), comprising of the cost function for the knee joint, S_k , and the cost function for the ankle joint, S_{a}.

$$S(t) = [S_k \quad S_a]^T$$

$$S_k(t) = -\frac{1}{2}\left(\frac{\theta_{rk} - \theta_k}{\theta_{mk}}\right)^2 - \frac{1}{2}\left(\frac{\dot{\theta}_{rk} - \dot{\theta}_k}{\dot{\theta}_{mk}}\right)^2$$

$$S_a(t) = -\frac{1}{2}\left(\frac{\theta_{ra} - \theta_a}{\theta_{ma}}\right)^2 - \frac{1}{2}\left(\frac{\dot{\theta}_{ra} - \dot{\theta}_a}{\dot{\theta}_{ma}}\right)^2 \tag{6.5}$$

where $\theta_{rk}, \theta_{ra}, \dot{\theta}_{rk}, \dot{\theta}_{ra}$ are desired angular positions and velocities for knee and ankle joints. $\theta_k, \theta_a, \dot{\theta}_k, \dot{\theta}_a$ are actual angular positions and velocities for knee and ankle joints. $\theta_{mk}, \theta_{ma}, \dot{\theta}_{mk}, \dot{\theta}_{ma}$ are the maximal values for position and velocities for knee and ankle joints.

To assess the controller's overall impact, we calculate the system's long-term cost $'J(t)'$ by aggregating the short-term costs defined in equation (10) over time for the prosthetic system:

$$J(t) = S(t+1) + \alpha S(t+2) + \alpha^2 S(t+3) + \cdots$$
$$= S(t+1) + \alpha J(t+1) \quad (6.6)$$

In which, α $(0 < \alpha < 1)$, is a discount factor and *S(t)* is the short-term cost function.

Accurate approximation of the long-term cost function can be achieved using a critic radial basis function (RBF) neural network, depicted in Figure 5.1, renowned for its ability to model nonlinear functions effectively within a single hidden layer.

The output of the optimal critic RBF network can be used to estimate the long term cost for the prosthetic controller.

$$J(\mathrm{t}) = W_c{}^T h_c(x_c) + \varepsilon_c, \quad (6.7)$$

Where, $h_{c(j)} = exp^{-\frac{|x_c - \mu_j|}{b_j}}; j = 1,2,3,4, \ldots k$

and x_c is the input to the network. μ_j, b_j is the center and width of the gaussian of the neural net 'k'. W_c represents the ideal weight of the critic network and ε_c is the error in approximating the long term cost. The critic network generates $\hat{J}(t)$ as an approximation of the long-term cost function *J(t).* Approximation of long-term cost function with an RBF NN is defined as:

$$\hat{J}(\mathrm{t}) = \widehat{W}_c{}^T \mathrm{h}_c(x_c) \quad (6.8)$$

Where, $\widehat{W}_c = W_c - \widetilde{W}_c$; $\widehat{W}_c$ is the estimated critic network weight.

In the proposed control structure, critic network inputs are:

$$x_c = \left[e_k\ e_a\ \dot{e}_k\ \ \dot{e}_a\ \theta_k\ \theta_a\ \dot{\theta}_k\ \ \dot{\theta}_a\ \hat{f}_k(x_{\mathrm{Ac}})\hat{f}_{\mathrm{a}}(x_{\mathrm{Ac}})\right] \tag{6.9}$$

in which, $e_k, e_a, \dot{e}_k, \dot{e}_a$ are tracking errors of the knee and ankle joints and their corresponding derivatives. $\theta_k\ \theta_a\ \dot{\theta}_k\ \ \dot{\theta}_a$ are knee and ankle joints' calculated angles and velocities. $\hat{f}_k(x_{\mathrm{Ac}}), \hat{f}_{\mathrm{a}}(x_{\mathrm{Ac}})$ are non-linearities estimation of knee and ankle joints by actor network. System nonlinearities f can be accurately estimated by:

$$f(x_{\mathrm{Ac}}) = W_a{}^T h_{Ac}(x_{\mathrm{Ac}}) + \ \varepsilon_a \tag{6.10}$$

$$\text{Where, } h_{Ac(j)} = exp^{-\frac{|x_{\mathrm{Ac}} - \mu_j|}{b_j}};\ j = 1,2,3,4, \ldots k$$

and 'x_{Ac}' is the input to the actor network. $'\mu_j'$, $'b_j'$ is the center and width of the gaussian of the neural net 'k'. 'W_a' represents the optimal weight of the actor network and $'\varepsilon_{\mathrm{a}}'$ is a very small value.

Approximation of the non linearities by RBF actor NN is :

$$\hat{f}(x_{\mathrm{Ac}}) = \widehat{W}_a{}^T \mathrm{h}_{Ac}(x_{\mathrm{Ac}}) \tag{6.11}$$

Where, $\widehat{W}_a$ is the approximation of the optimal actor network weight.

$$f(x_{\mathrm{Ac}}) - \hat{f}(x_{\mathrm{Ac}}) = \widetilde{W}_a{}^T \mathrm{h}_{Ac}(x_{\mathrm{Ac}}) + \ \varepsilon_a \tag{6.12}$$

The backpropagation error for critic network $'e_c'$ is defined as:

$$e_c = \left[\hat{\jmath}\,(t-1) - S(t)\right] - \alpha\hat{\jmath}(t) \tag{6.13}$$

Update laws of the critic network are defined as:

$$\dot{\widehat{W}}_c = \alpha F_c h_c r^T - \kappa F_c \|e_c\| \widehat{W}_c \tag{6.14}$$

where 'α' is the discount factor, and F_c and κ are design parameters. r, e_c are filtered tracking error and critic network's backpropagation error respectively. Further, h_c for critic network can be computed using (6.7).

The action network compensates for the nonlinear dynamics in knee and ankle joints, thereby improving tracking accuracy and reducing short-term costs. The estimated long-term cost from the critic network is utilized to modify the current 'action' generated by the action network. Consequently, this process enhances knee and ankle trajectory tracking while reducing long-term costs. For learning and estimating nonlinearities with the actor network, we utilize the RBF network described in equation (6.10). The inputs to the actor network are:

$$x_{\mathrm{Ac}} = \left[e_k\ e_a\ \dot{e}_k\ \ \dot{e}_a\ \theta_k\ \theta_a\ \dot{\theta}_k\ \ \dot{\theta}_a\ \ \ddot{\theta}_k\ \ddot{\theta}_a\right] \tag{6.15}$$

Where, $e_k, e_a, \dot{e}_k, \dot{e}_a$ are knee and ankle joints' tracking errors and their derivatives. $\theta_k, \theta_a, \dot{\theta}_k, \dot{\theta}_a, \ddot{\theta}_k, \ddot{\theta}_a$ are knee and ankle joints' calculated angles, velocities and accelerations.

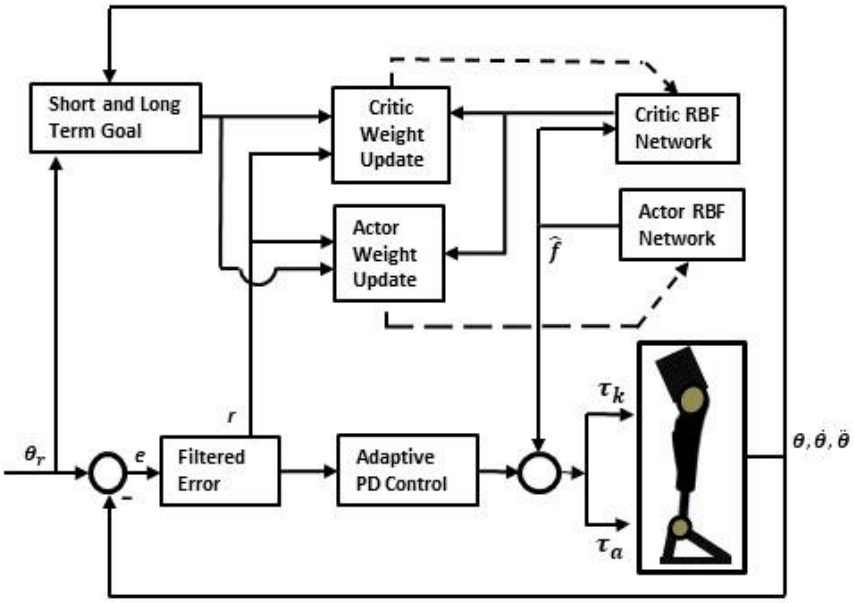

Figure 6.1: NDP control structure for prosthetic leg.

The system input is modified by the actor network to minimize the long-term cost function. In order to find out a control goal which reduces the infinite horizon long term system cost to minimum possible value, we define an ultimate control goal $U_c(t)$. The ultimate control goal $U_c(t) = 0$, which is the long-term cost approximation of $\hat{J}(t)$.

Back propagation error for actor network is given as follows:

$$e_{Ac} = U_c(t) - \hat{J}(t) \tag{6.16}$$

The tuning rule for actor network is given as:

$$\dot{\hat{W}}_a = F_a h_{Ac} r^T - \kappa F_a \| e_{Ac} \| \hat{W}_a \tag{6.17}$$

In which, F_a and κ are design parameters. r, e_{Ac} are filtered tracking error and actor network's backpropagation error respectively. h_{Ac} for actor network can be computed using (6.11)

The outline of the control agorithm is shown below.

Algorithm 1: NDP controller implementation

1. Generate desired trajectory: $\theta_r, \dot{\theta}_r, \ddot{\theta}_r$
2. Initiate $\theta, \dot{\theta}, \ddot{\theta} \rightarrow \leq 0.1$. long term cost estimation at $\hat{J}(t) = 0$
3. Solve $\theta, \dot{\theta}, \ddot{\theta}$ from the system dynamics
4. Calculate short term cost: S(t), and long-term cost: *J(t-1)*
5. Calculate the error terms: e, $\dot{e}$, and filter tracking error: r
6. Calculate critic network error: e_c
7. Update critic network weight*:* $\widehat{W}_c$
8. Estimate long term cost: $\hat{J}(t)$
9. Calculate actor network error: e_a
10. Update actor network weight: $\widehat{W}_a$
11. Estimate the nonlinearities in the system $\hat{f}(x_{\mathrm{Ac}})$ with actor network
12. Calculate system input torque to the system

Theorem VII.I: The control law $\tau = \hat{f}(\mathrm{x}) + K_v \mathrm{r} - \upsilon$, along with the actor and critic network weight update laws $\dot{\widehat{W}}_c = \alpha F_c h_c r^T - \kappa F_c \| e_c \| \widehat{W}_c$, and $\dot{\widehat{W}}_a = F_a h_{Ac} r^T - \kappa F_a \| e_{Ac} \| \widehat{W}_a$ ensures that the tracking error $r(t) = \dot{e} + \lambda e$ is ultimately bounded. Further, the cumulative long-term cost *J(t)* is also bounded.

Proof :

Consider the Lyapunov function

$L=\frac{1}{2}r^T Mr + \frac{1}{2}tr\left(\widetilde{W}_a^T F_a^{-1}\widetilde{W}_a\right)+\frac{1}{2}tr\left(\widetilde{W}_c^T F_c^{-1}\widetilde{W}_c\right)$ where, where, M is symmetric positive definite, $F_a = F_a^T > 0, F_c = F_c^T > 0.$ $\widetilde{W}_a = W_a - \widehat{W}_a$; and $\widetilde{W}_c = W_c - \widehat{W}_c$; W_a and W_c are ideal actor and critic network weights for estimating cost function and system input. Taking the the derivative of the lyapunov equation we find:

$$\dot{L}= r^T M\dot{r} + \frac{1}{2}r^T \dot{M}r + tr\left(\widetilde{W}_a^T F_a^{-1}\dot{\widetilde{W}}_a\right) + tr\left(\widetilde{W}_c^T F_c^{-1}\dot{\widetilde{W}}_c\right)$$

Using (6.3), (6.4), and (6.12)we can find:

$$\dot{L}= -r^T K_v \mathrm{r} + \frac{1}{2}r^T(\dot{M} - 2V)r + r^T\left(\widetilde{W}_a^T \mathrm{h_{Ac}} + \upsilon + \varepsilon\right) - tr\left(\widetilde{W}_a^T F_a^{-1}\dot{\widetilde{W}}_a\right)$$

$$- tr\left(\widetilde{W}_c^T F_c^{-1}\dot{\widetilde{W}}_c\right)$$

Due to skew symmetric characteristic, $\dot{M} - 2V = 0$;

Using (6.14), and (6.17) we can write:

$$\dot{L}= -r^T K_v \mathrm{r} + r^T\left(\widetilde{W}_a^T \mathrm{h_{Ac}}\right) + r^T(\upsilon + \varepsilon_a) - tr\left(\widetilde{W}_a^T F_a^{-1}\left(\mathrm{F}_a \mathrm{h_{Ac}} \mathrm{r}^{\mathrm{T}} - \kappa \mathrm{F}_a \|\mathrm{e_{Ac}}\| \widehat{W}_{\mathrm{a}}\right)\right) -$$

$$tr\left(\widetilde{W}_c^T F_c^{-1}\left(\alpha \mathrm{F}_c \mathrm{h_c} \mathrm{r}^{\mathrm{T}} - \kappa \mathrm{F}_c \|\mathrm{e_c}\| \widehat{W}_{\mathrm{c}}\right)\right)$$

$$\dot{L} = -r^T K_v \mathrm{r} + r^T\left(\widetilde{W}_a^T \mathrm{h_{Ac}}\right) + r^T(\upsilon + \varepsilon_a) - tr\left(\widetilde{W}_a^T \mathrm{h_{Ac}} \mathrm{r}^{\mathrm{T}}\right) + \kappa\, tr\left(\|\mathrm{e_{Ac}}\| \widehat{W}_{\mathrm{a}}\right) - \alpha$$

$$tr\left(\widetilde{W}_c^T \mathrm{h_c} \mathrm{r}^{\mathrm{T}}\right) + \kappa\, tr\left(\widetilde{W}_c^T \|\mathrm{e_c}\| \widehat{W}_{\mathrm{c}}\right)$$

Using υ from (9) gives :

$$\dot{L} = -r^T K_v \mathrm{r} + r^T(-\acute{\upsilon}\mathrm{sgn}(\mathrm{r}) + \varepsilon_a)) + \kappa\, tr\left(\|\mathrm{e_{Ac}}\| \widehat{W}_{\mathrm{a}}\right) - \alpha\, tr\left(\widetilde{W}_c^T \mathrm{h_c} \mathrm{r}^{\mathrm{T}}\right) + \kappa$$

$$tr\left(\widetilde{W}_c^T \|\mathrm{e_c}\| \widehat{W}_{\mathrm{c}}\right)$$

Here, 1st and 4th terms are negative.

2nd term $r^T(-\acute{\upsilon}\mathrm{sgn}(\mathrm{r})+\varepsilon))$ = r^T (ε) + $r^T(-\acute{\upsilon}\mathrm{sgn}(\mathrm{r}))$ = r^T (ε) – $\|r\|$ $(\acute{\upsilon})\leq 0$, when $\acute{\upsilon} > \varepsilon$

3rd term, $\kappa\, tr\,(\|\mathrm{e_{Ac}}\|\widehat{W}_{\mathrm{a}})$ = $\kappa\, tr\,(\|\mathrm{e_{Ac}}\|(W_a-\widetilde{W}_a))$ <0 , when $\widetilde{W}_a > W_a$ or, $\widetilde{W}_a > W_{ab}$

Similarly 5th term, $\kappa\, tr\left(\widetilde{W}_c^T\|\mathrm{e_c}\|\widehat{W}_{\mathrm{c}}\right)$ = $\kappa\, tr(\widetilde{W}_c^T\|\mathrm{e_c}\|(W_c-\widetilde{W}_c))$) <0 , when $\widetilde{W}_c > W_c$ or, $\widetilde{W}_c > W_{cb}$.

Therefore, there exist non-negative bounds r_b, W_{ab}, W_{cb}, such that $\dot{L}$ is negative definite whenever $r>r_b$, $\widetilde{W}_a > W_{ab}$, $\widetilde{W}_c > W_{cb}$, where r_b is the bound for filtered tracking error r, and W_{ab}, and W_{cb} are the upper bound for actor and critic network estimation errors $\widetilde{W}_a$ and $\widetilde{W}_c$. Since the filtered tracking error system in (6.1) is Hurwitz, this implies that the tracking error and its derivatives are also bounded and can be made arbitrarily small by selecting the parameter λ.

Further, these bounds can be made small by proper choice of design parameters (feedback gains and the gains used in the weight updates). For bounded network weights, the long term cost will also be bounded as the to-go cost is a function of optimum network weights.

6.3 Numerical Examples

The performance of the proposed control strategyis demonstrated through several simulation examples that represent variations in gait experienced by an user during daily activities. In these simultations, it is assumed that the prosthetic device is fitted on a healthy male of height 1.78 meters and weighing 90.7 kilograms. Corresponding gait data from a similar intact individual is first collected and analyzed. Based on the normal cadence of an individual, nominal trajectories for knee and ankle joints are then approximated using

parameterization of gait data collected from human subjects [91]. From Figure 6.2, it can be seen that the approximate displacement profile for the knee is close to the actual knee profile of an individual.

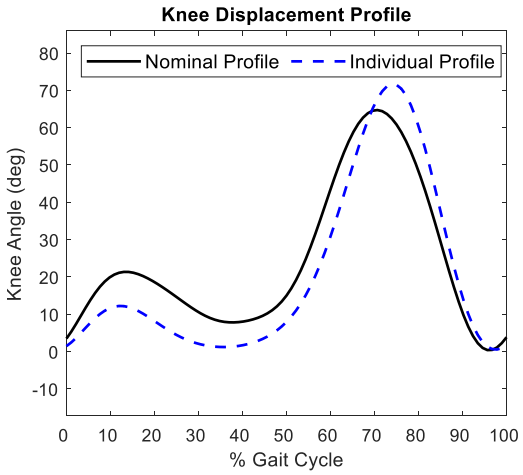

Figure 6.2 : Nominal and individual's knee displacement profiles.

Further, data in Table 6.1 shows that at each phase of the gait, the approximate displacement profile is within a small bound of the actual displacement profile seen in a similar intact individual. Therefore, in these simulation examples, the stance time is first measured from the intact side and then used to generate a desired displacement profiles using the parametrization of nominal gait.

Table 6.1: Knee, Ankle and Foot angles for nominal and individual's gait profiles during stance phase. Nom. = Nominal, Ind. = Individual. HS=Heel Strike, FF = Foot Flat, MS = Mid Stance, HO = Heel Off, TO = Toe Off.

Gait Ph.	Knee Angle		Ankle Angle		Foot Angle	
	Nom.	Ind.	Nom.	Ind.	Nom.	Ind.
HS	3.48	1.47	-1.00	-4.67	17.35	7.68
FF	19.68	11.61	-2.46	1.64	0.00	1.05
MS	14.63	4.47	6.43	6.43	0.58	-1.09
HO	9.04	2.85	9.70	12.11	-9.99	-4.18
TO	58.39	62.69	-15.94	-6.84	-81.60	-71.19

The simulation experiments were designed to study the performance with respect to:

a) tracking the desired knee and ankle joint profiles with variation in gait dynamics,

b) orientation of the foot relative to the ground during a gait,

c) monte carlo simulations to analyze gait assymetry,

d) adaptability to variable walking speed.

e) robustness to measurement and actuator noises, and

f) small long-term to go cost and neural network's stable performance.

All of these experiments are performed to investigate controller's ability to achieve near natural gait. Achieving gait symmetry requires the prosthetic foot to make contact with the ground at the same instant in the gait cycle as the intact foot, i.e. heel strike should be similar on the intact and prosthetic side. Further, the instant for 'Foot-Flat' and 'Toe-off' also have to be similar. Another challenge that has to be addressed is the ability of the controller to adjust to different gait requirements. The following simulations address these aspects of performance.

6.3.1 Tracking performance of desired joint trajectories and foot orientation.

Misalignment of the joints or improper foot position during gait limits the mobility of a person. Hence, knee and ankle profiles tracking simulations along with foot position during a gait have been performed. The parameters for model dynamics and the design values are given in the Appendices. The tracking performance of the knee and ankle joints with variation in gait dynamics is shown in Figure 6.3- Figure 6.10. Figure 6.3 shows that the proposed NDP controller is able to track the nominal knee and ankle profiles (medium cadence) with very little error. In Figure 6.4-Figure 6.8, tracking errors for knee and ankle angle have been plotted considering slow cadence, fast cadence, 25% increased ground

reaction force, 20% increased disturbance torques and measurement noise in the system dynamics.

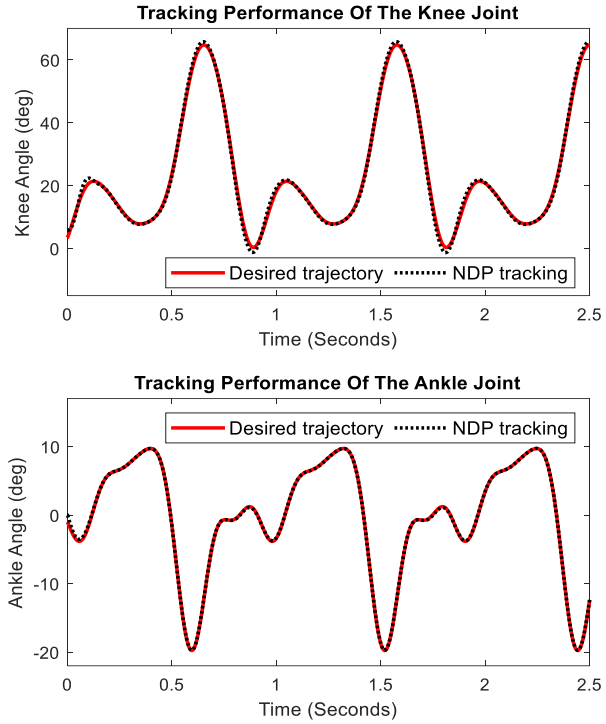

Figure 6.3: Tracking performance of knee, and ankle joints in medium cadence.

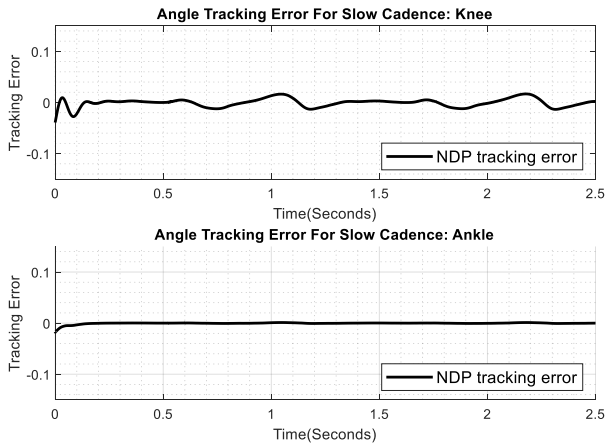

Figure 6.4: Tracking performance of knee, and ankle joints for slow cadence.

From the error plots, it is observed that propsed controller keeps the tracking error very close to zero even with significant amount of variation in the system dynamics. Actor network is able to accurately estimate the non-linearities associated with knee and ankle joints. As a result, the foot position is maintained close to the desired position during different gait phases.

Figure 6.9 shows the Mean Square Error (MSE) for knee-ankle joint tracking for NDP, NN, and PD controllers in medium cadence. The results indicate that NDP outperfroms NN and PD controllers in terms of joint tracking performance. It is observed in Figure 6.10 that the foot position in both stance and swing phase of the prosthesis is similar to that of an intact leg. Further during the 'Foot-Flat (FF)' to 'Mid- Stance (MS)' phase, the controller is able to maintain desired foot position identical to an intact leg. This implies that the stance on both intact and prosthetic side is similar leading to the conclusion that the weight bearing is similar on both sides.

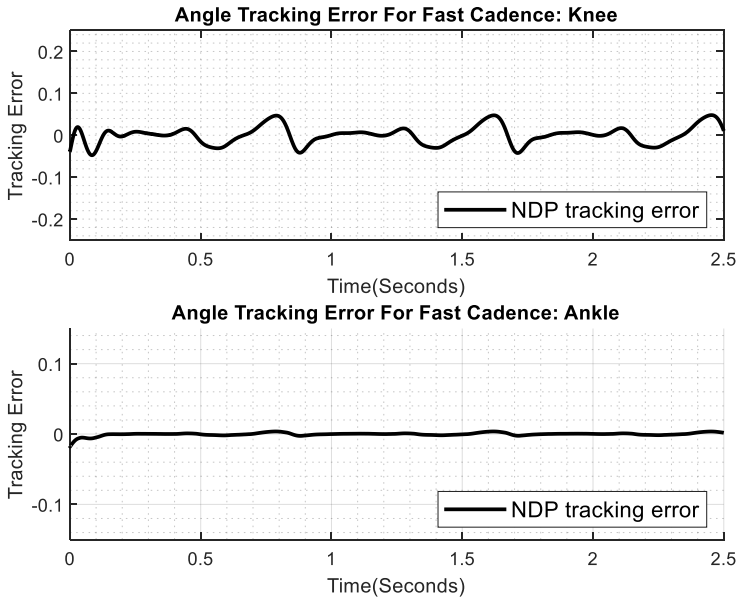

Figure 6.5: Tracking performance of knee, and ankle joints for fast cadence.

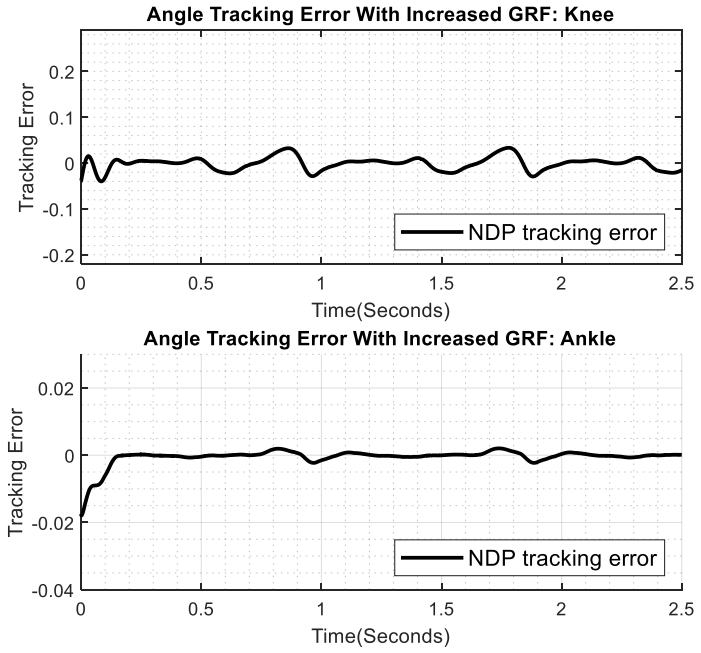

Figure 6.6: Tracking performance knee, and ankle joints with 25% increased GRF.

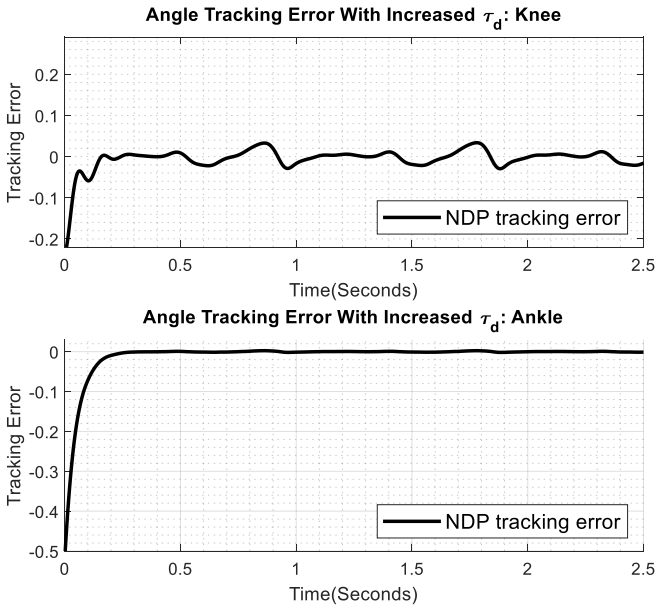

Figure 6.7: Tracking performance knee, and ankle joints with 20% increased disturbance torque.

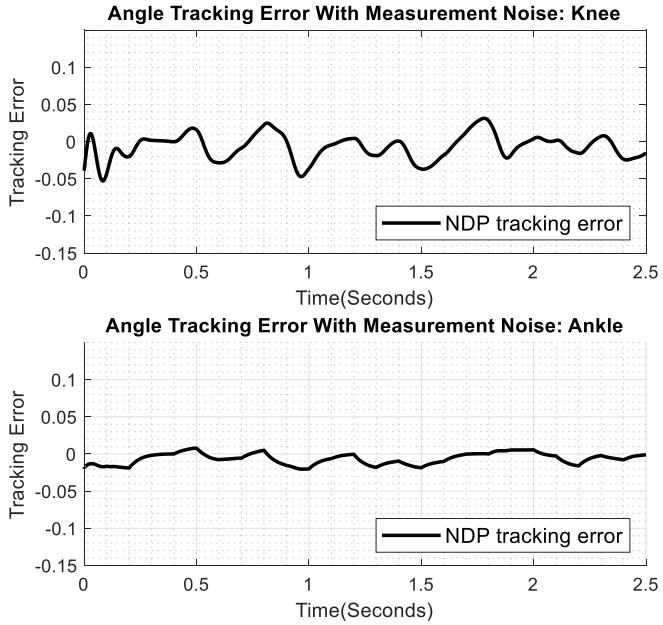

Figure 6.8: Tracking performance knee, and ankle joints with measurement noise.

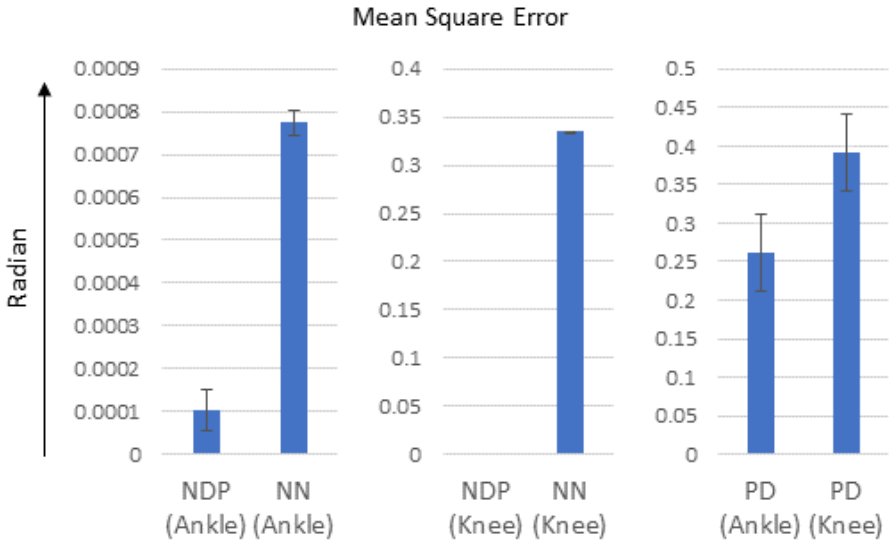

Figure 6.9: MSE error for Knee- Ankle joint tracking for NDP, NN, and PD in medium cadence.

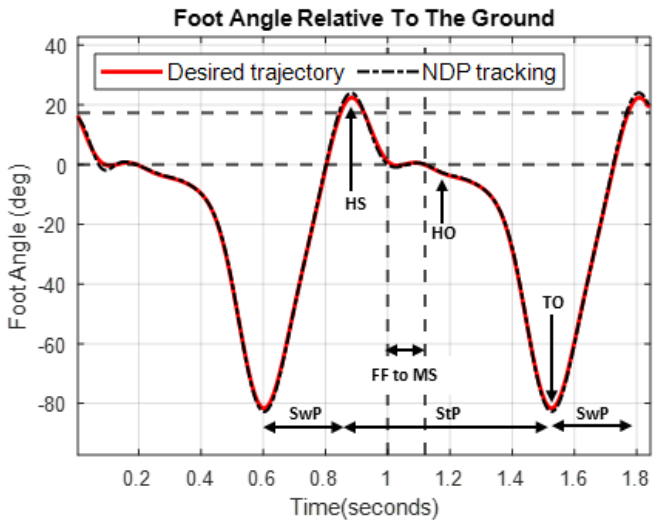

Figure 6.10: Foot position of the prosthetic leg with NDP controller. (HS=Heel Strike, FF = Foot Flat, MS = Mid Stance, HO = Heel Off, TO = Toe Off, SwP = Swing Phase, StP = Stance Phase).

6.3.2 Analyze gait assymetry using monte-carlo simulations.

Gait symmetry of a person depends on the support time during the stance period of a gait. To analyze the performace of the propsed controller in terms of support time for an amputee monte carlo simulation has been performed for 1000 trials considering walking dynamics (speed, noise, ground reaction torque) as variables in each trial. In Figure 6.11, it is observed that mean foot flat (FF) time error for the propsed controller is about 6 milliseconds, whereas for adaptive NN it is 6.7 milliseconds and for PD it is 149 milliseconds. Also, in the heel off phase mean error for proposed controller is about 2 milliseconds, whereas for adaptive NN it is about 5 milliseconds and for PD it is 154 milliseconds. As the time difference between Heel off (HO) and Foot flat (FF) phases define the support time, from the obtaned results it is concluded that the proposed controller performes better to reduce gait assymetry than the traditional controllers.

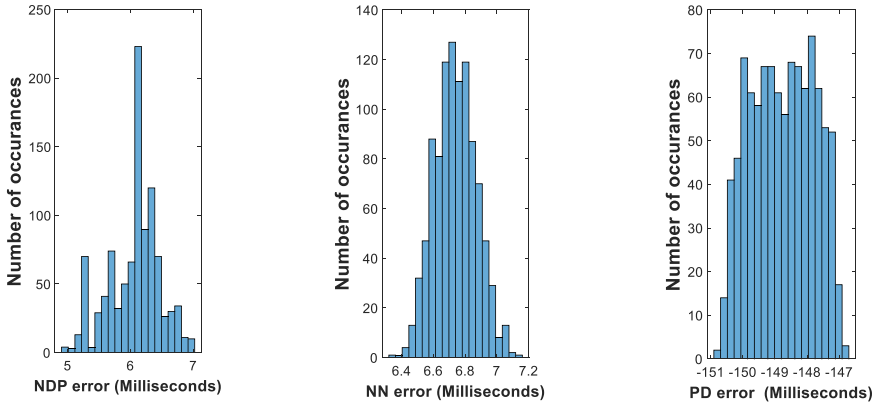

(a) Loading Response (LR) error

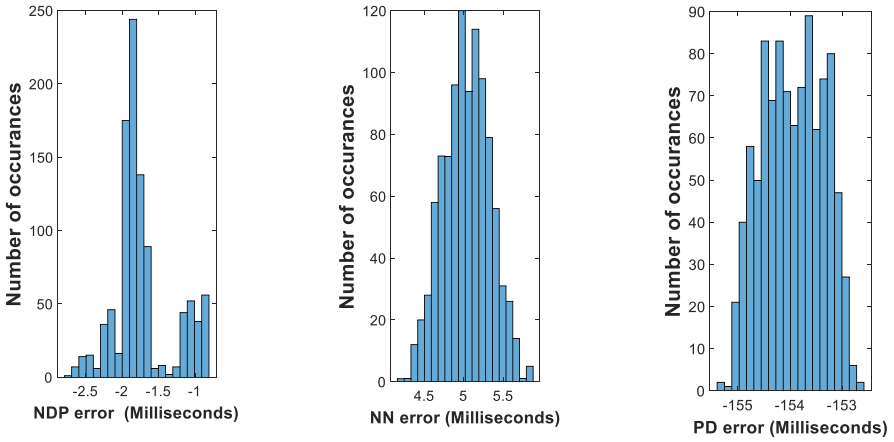

(b) Terminal Swing (TS) error

Figure 6.11: Monte Carlo Simulation error plot at (a) Loading response, and (b) Terminal Swing instances for PD, NN, and NDP controller. Total 1000 occurrences.

6.3.3 Long term "to go" cost

It is an established fact that a person's gait is quasi-periodic [92]. To check the proposed controller's adaptibility with irregular strides of a person and immunity of the designed mechanism againts mechanical noises simulations (d), (e), (f) have been performed. Several medical experiments have been conducted to study the long term effects of prosthesis on patient's health [93, 94]. These simulations have been designed in terms of long term to go cost which can be found by accumulating short term costs in each instances of the gait. Hence these simulations give the visibilty of gait assymetry reduction for long term usage of the prosthesis.

To check the effect of variations in walking speed, we calculate the long-term costs associated with knee and ankle joints with the proposed control model. We have tabulated the long-term cost for 3 different gaits with medium, slow and fast cadence (Table 2). To compare the proposed controller's performance with traditional PD and adaptive NN based

controllers we perform simulation with same set up and observe that NDP based controller outperforms both PD and Adaptive NN controllers (Table 2).

Table 6.2: Long-term cost for different walking cadence.

Gait Type	Joint	PD	Adaptive NN	NDP
Medium Cadence	Ankle joint	1.05	0.4694	0.0082
	Knee joint	5.05	1.3513	0.0083
Slow Cadence	Ankle joint	0.65	0.3728	0.0055
	Knee joint	5.59	0.9657	0.0055
Fast Cadence	Ankle joint	1.8698	0.6981	0.0984
	Knee joint	6.0650	2.0096	0. 0985

To investigate the performance of the proposed controller with noise, uniformly distributed measurement and actuator noises are added into the system. System is affected with 2% added measurement noise to θ and $\dot{\theta}$ and 20% actuator noise to τ. Considering the individual is walking in a medium cadence, we analyze the long-term cost for the proposed NDP, PD and Adaptive NN controllers in noisy environment. It is observed from the simulation results tabulated in Table 6.3 that NDP based controller is less susceptible to added noise and performs better than the rest controllers in terms of long-term cost.

Table 6.3: Long term cost with increasing measurement and actuator noise.

Noise	Joint	PD	Adaptive NN	NDP
	Ankle joint	1.34	0.4845	0.0227

2% measurement Noise	Knee joint	5.5678	1.3868	0.0127
20% actuator noise	Ankle joint	1.2686	0.4917	0.0241
	Knee joint	5.2235	1.1219	0.0242

6.4 Conclusions

In this chapter, a novel neuro-dynamic control approach for above-knee prosthetic system was developed to reduce gait asymmetry and achieve near natural gait. Using a filtered tracking error system and an actor-critic network, the controller was shown to be able to track synthesised displacement profiles for the knee and ankle joints while reducing the long-term cost. As a result, the performance of the controller improves after each step, i.e., after each stance phase of the gait. Data collected in the laboratory indicates that the synthesised gait profiles are close to the knee and ankle displacements in an intact individual while walking at self-selected pace. Simulation results demonstrate that the knee and ankle joints, as well as the angle the foot makes with the ground track the corresponding profiles on the intact side, thereby improving stance and reducing assymetry.

Chapter 7 CONCLUSIONS AND FUTURE RESEARCH

The challenges faced by individuals with transfemoral amputation was addressed in this dissertation through the development of an intelligent prosthetic leg capable of real-time adaptation to user gait. By studying the interface between the residual limb and the prosthetic socket, and the activity of residual muscles during gait, this research has shed light on possible ways to improve gait symmetry. Most works in literature focus on stability and limited mobility in individuals with amputation, and seldom on the resulting gait. This is an important limitation in the current state of the art as asymmetric gait can affect the mobility in the short term and the health of the individual in the long term.

Key findings include the successful validation of the transfemoral osteomyoplastic amputation (OTFA) procedure, providing evidence of its effectiveness in supporting body weight during gait and retaining muscle activity in the residual limb. This is the first time where the amputation effect for OTFA has been studied not only for residual limb but also for intact limb.

By leveraging these insights, the research also pioneered the development of learning-based control strategies capable of adaptively compensating for changing knee-ankle dynamics, thereby reducing gait asymmetry, and improving stability. The integration of actual gait data into the control framework marks a significant advancement in the field, promising more natural and efficient prosthetic gait patterns.

7.1 Future Works and Limitations

While the research presented in this dissertation marks a significant advancement in the field of prosthetic technology for individuals with transfemoral amputation (TFA), there remain several avenues for further exploration and improvement. This section outlines potential future works and acknowledges the limitations of the current research as following:

1. *Refinement of Control Framework through Mechanical Testing:* The control framework developed in this research relied on modeling and simulation to evaluate prosthetic performance. While promising, future works should focus on further validation through mechanical testing. Building and testing prototype prosthetic feet with the desired rigidity, mobility, and power characteristics would provide valuable insights into the practical implementation of the control strategies. Additionally, real-world testing on human subjects would help assess the robustness and effectiveness of the control framework in diverse gait conditions.

2. *Dynamical Model Refinement and Real-Time Gait Analysis:* To enhance the accuracy and effectiveness of the control framework, future research should focus on refining the dynamical model of the knee-ankle joint during gait. This refinement could be achieved through mathematical modeling and calibration with actual gait measurements. Furthermore, real-time intent recognition techniques should be developed to improve the accuracy of gait recognition and parameterization of gait patterns. Additionally, methods for real-time approximation of ground reaction torque could be explored to provide more accurate feedback for the control algorithms.

5. *Testing and Optimization of Controlled Prosthetic Foot:* While the proposed control strategies show promise in reducing gait asymmetry and improving stability, further testing and optimization of the controlled prosthetic foot are necessary. Mechanical property testing should be conducted to ensure that the prototype leg meets the required specifications in terms of durability, responsiveness, and safety. Quantitative gait analysis experiments should be performed to assess the performance of the controlled prosthetic legs under various gait conditions and environments.

6. *Extension to Bilateral OTFA and other Transfemoral Amputations:* The scope of future research could be extended to include individuals with bilateral OTFA as well as other forms of transfemoral amputation. By studying a broader population of amputees, researchers can gain insights into the unique challenges and requirements associated with different amputation levels and configurations. This expanded scope would contribute to the development of more versatile and adaptable prosthetic technologies that cater to a diverse range of user needs.

7. *Long-Term Health Implications and User-Centered Design:* In addition to technical advancements, future research should also consider the long-term health implications of prosthetic interventions. Longitudinal studies tracking the physical health, mobility, and quality of life outcomes of individuals using intelligent prosthetic legs would provide valuable insights into the effectiveness and sustainability of these technologies. Furthermore, user-centered design principles should be incorporated into the development process to ensure that prosthetic devices meet the functional, ergonomic, and psychosocial needs of their users.

Addressing these limitations and pursuing the outlined future works will contribute to

the continued advancement of prosthetic technology for individuals with transfemoral amputation, ultimately enhancing their mobility, function, and quality of life.

APPENDICES

From (4.1) the dynamic model of the prosthetic leg is defined as:

$$M(\theta)\ddot{\theta} + V(\theta,\dot{\theta})\dot{\theta} + G(\theta) + F(\dot{\theta}) + \tau_d = \tau + \tau_G$$

Dynamics Matrices: $M(\theta) = \begin{bmatrix} M_{ka(1,1)} & M_{ka(1,2)} \\ M_{ka(2,1)} & M_{ka(2,2)} \end{bmatrix}$

$$M_{(1,1)} = (m_k + m_a)l_k^2 + m_a l_a^2 + 2m_a l_k l_a \cos\theta_a$$

$$M_{(1,2)} = M_{(2,1)} = m_a l_a^2 + m_a l_k l_a \cos\theta_a$$

$$M_{(2,2)} = m_a l_a^2$$

$$V(\theta,\dot{\theta}) = \begin{bmatrix} -m_a l_k l_a(2\dot{\theta}_k\dot{\theta}_a + \dot{\theta}_a^2)\sin\theta_a \\ m_a l_k l_a \dot{\theta}_k^2 \sin\theta_a \end{bmatrix}$$

$$G(\theta) = \begin{bmatrix} (m_k + m_a)g l_k \cos\theta_k + m_a g l_a \cos(\theta_k + \theta_a) \\ m_a g l_k \cos(\theta_k + \theta_a) \end{bmatrix}$$

$$F_{ka}(\theta) = \dot{\kappa_{d(\theta)}} sgn(\dot{\theta})$$

$\theta = [\theta_k \quad \theta_a]^T$; $\dot{\theta} = [\dot{\theta}_k \quad \dot{\theta}_a]^T$; $\ddot{\theta} = [\ddot{\theta}_k \quad \ddot{\theta}_a]^T$.

$\tau_d = [\tau_k \quad \tau_a]^T$; $\tau_G = [\tau_{G(k)} \quad \tau_{G(a)}]^T$; $\tau = [\tau_k \quad \tau_a]^T$

Subscripts ‘k’ and ‘a’ denotes knee and ankle joints respectively.

Table A.1: Plant parameters.

m_k $(Knee\ to\ ankle\ link\ (Shank) mass)$	2.63 kg
m_a $(Ankle\ and\ foot\ mass)$	0.82 kg
l_k $(Knee\ to\ ankle\ joint\ length)$	0.19 m
l_a $(Ankle\ joint\ to\ heel\ length)$	0.06 m

$g\ (Gravitational\ acceleration)$	9.8 ms-2
$\kappa_{d(\theta)}\ (Dynamic\ Friction\ Coefficient)$	0.2

Assuming that the individual is an average male weighing 73.0 kilograms (kgs) and of height 1.741 meters (m), m_k, m_a, l_k, l_a are collected from [95]

Table A.2: Design values.

$\lambda(Design\ parameter)$	6
$K_v(Design\ parameter)$	4
ύ$(Design\ Parameter)$	0.3
α (Discount factor)	0.97
$F_c = F_a$ (NN tuning gain)	$\begin{bmatrix} 22 & 0 \\ 0 & 22 \end{bmatrix}$
κ (NN design parameter)	1
$\bar{k}$ (Spring coefficient to measure GRF)	2×10^6 Nm^{-1}
Spe (Spring exponent to measure GRF)	2.2
μ̄ (Friction coefficient to measure GRF)	0.2
Network structure for actor and critic	Input node: 10 Hidden layer: 30 Output layer: 2

REFERENCES

[1] L. Y. T. Gorden, Y. F. Ariel, H. Pei, M. Lingyan, N. G. Y. Zhen, and N. Graves, "Decision-making for early major amputation in selected diabetic foot ulcer patients with peripheral vascular disease," *Health Care Science,* vol. 1, no. 2, pp. 58-68, 2022, doi: 10.1002/hcs2.17.

[2] D. P. Laroche, S. B. Cook, and K. Mackala, "Strength Asymmetry Increases Gait Asymmetry and Variability in Older Women," *Medicine & Science in Sports & Exercise,* vol. 44, no. 11, pp. 2172-2181, 2012, doi: 10.1249/MSS.0b013e31825e1d31.

[3] R. Gailey, K. Allen, J. Castles, J. Kucharik, and M. Roeder, "Review of secondary physical conditions associated with lower-limb amputation and long-term prosthesis use.," *Journal of rehabilitation research and development,* vol. 45 1, pp. 15-29 %3, 2008.

[4] P. G. Adamczyk and A. D. Kuo, "Mechanisms of Gait Asymmetry Due to Push-Off Deficiency in Unilateral Amputees," *IEEE Transactions on Neural Systems and Rehabilitation Engineering,* vol. 23, no. 5, pp. 776-785, 2015, doi: 10.1109/TNSRE.2014.2356722.

[5] K. Ziegler-Graham, E. J. MacKenzie, P. L. Ephraim, T. G. Travison, and R. Brookmeyer, "Estimating the Prevalence of Limb Loss in the United States: 2005 to 2050," (in "English (US)"), *Archives of Physical Medicine and Rehabilitation,* vol. 89, no. 3 , %4, pp. 422--429, mar 2008, doi: 10.1016/j.apmr.2007.11.005.

[6] I. C. Lee, M. Liu, M. D. Lewek, X. Hu, W. G. Filer, and H. Huang, "Toward Safe Wearer-Prosthesis Interaction: Evaluation of Gait Stability and Human Compensation Strategy Under Faults in Robotic Transfemoral Prostheses," *IEEE Transactions on Neural Systems and Rehabilitation Engineering,* vol. 30, pp. 2773-2782, 2022, doi: 10.1109/TNSRE.2022.3208778.

[7] R. Sharma, G. P., B. S., and J. D., "Performance assessment of fuzzy logic control approach for MR damper based-transfemoral prosthetic leg," *IEEE Transactions on Artificial Intelligence,* pp. 1-1, 2021, doi: 10.1109/TAI.2021.3106884.

[8] Y. Feng and Q. Wang, "Combining Push-Off Power and Nonlinear Damping Behaviors for a Lightweight Motor-Driven Transtibial Prosthesis," *IEEE/ASME Transactions on Mechatronics,* vol. 22, no. 6, pp. 2512-2523, 2017, doi: 10.1109/TMECH.2017.2766205.

[9] H. L. Bartlett, B. E. Lawson, and M. Goldfarb, "Design, Control, and Preliminary Assessment of a Multifunctional Semipowered Ankle Prosthesis," *IEEE/ASME Transactions on Mechatronics,* vol. 24, no. 4, pp. 1532-1540, 2019, doi: 10.1109/TMECH.2019.2918685.

[10] J. Camargo, K. Bhakta, K. Herrin, and A. Young, "Biomechanical Evaluation of Stair Ambulation Using Impedance Control on an Active Prosthesis," *Journal of Biomechanical Engineering,* vol. 145, no. 2, 2022, doi: 10.1115/1.4055759.

[11] B. Convens *et al.*, "Modeling, Design and Test-Bench Validation of a Semi-Active Propulsive Ankle Prosthesis With a Clutched Series Elastic Actuator," *IEEE Robotics and Automation Letters,* vol. 4, no. 2, pp. 1823-1830, 2019, doi: 10.1109/LRA.2019.2897993.

[12] R. S. T. Saini, H. Kumar, and S. Chandramohan, "Semi-active control of a swing phase dynamic model of transfemoral prosthetic device based on inverse dynamic model,"

Journal of the Brazilian Society of Mechanical Sciences and Engineering, vol. 42, no. 6, p. 294, May , day= 14 2020.

[13] J. T. Lee, H. L. Bartlett, and M. Goldfarb, "Design of a Semipowered Stance-Control Swing-Assist Transfemoral Prosthesis," *IEEE/ASME Transactions on Mechatronics,* vol. 25, no. 1, pp. 175-184, 2020, doi: 10.1109/TMECH.2019.2952084.

[14] M. A. McGeehan, P. G. Adamczyk, K. M. Nichols, and M. E. Hahn, "A Reduced-Order Computational Model of a Semi-Active Variable-Stiffness Foot Prosthesis," *Journal of Biomechanical Engineering,* vol. 143, no. 7, 2021, doi: 10.1115/1.4050456.

[15] T. Lenzi, M. Cempini, L. J. Hargrove, and T. A. Kuiken, "Design, Development, and Validation of a Lightweight Nonbackdrivable Robotic Ankle Prosthesis," *IEEE/ASME Transactions on Mechatronics,* vol. 24, no. 2, pp. 471-482, 2019, doi: 10.1109/TMECH.2019.2892609.

[16] H. Zhu, C. Nesler, N. Divekar, V. Peddinti, and R. D. Gregg, "Design Principles for Compact, Backdrivable Actuation in Partial-Assist Powered Knee Orthoses," *IEEE/ASME Transactions on Mechatronics,* vol. 26, no. 6, pp. 3104-3115, 2021, doi: 10.1109/TMECH.2021.3053226.

[17] P. Cherelle, V. Grosu, A. Matthys, B. Vanderborght, and D. Lefeber, "Design and Validation of the Ankle Mimicking Prosthetic (AMP-) Foot 2.0," *IEEE Transactions on Neural Systems and Rehabilitation Engineering,* vol. 22, no. 1, pp. 138-148, 2014, doi: 10.1109/TNSRE.2013.2282416 %13.

[18] K. R. Embry and R. D. Gregg, "Analysis of Continuously Varying Kinematics for Prosthetic Leg Control Applications," *IEEE Transactions on Neural Systems and Rehabilitation Engineering,* vol. 29, pp. 262-272, 2021, doi: 10.1109/TNSRE.2020.3045003.

[19] M. Pi *et al.*, "Biologically Inspired Deadbeat Control of Robotic Leg Prostheses," *IEEE/ASME Transactions on Mechatronics,* vol. 25, no. 6, pp. 2733-2742, 2020, doi: 10.1109/TMECH.2020.2990406.

[20] S. Gao, J. Mai, J. Zhu, and Q. Wang, "Mechanism and Controller Design of a Transfemoral Prosthesis With Electrohydraulic Knee and Motor-Driven Ankle," *IEEE/ASME Transactions on Mechatronics,* vol. 26, no. 5, pp. 2429-2439, 2021, doi: 10.1109/TMECH.2020.3040369.

[21] M. Li, X. Gao, Y. Wen, J. Si, and H. H. Huang, "Offline Policy Iteration Based Reinforcement Learning Controller for Online Robotic Knee Prosthesis Parameter Tuning," presented at the 2019 International Conference on Robotics and Automation (ICRA), 2019.

[22] T. K. Best, C. G. Welker, E. J. Rouse, and R. D. Gregg, "Data-Driven Variable Impedance Control of a Powered Knee–Ankle Prosthesis for Adaptive Speed and Incline Walking," *IEEE Transactions on Robotics,* pp. 1-19, 2023, doi: 10.1109/TRO.2022.3226887.

[23] Y. Lv, J. Xu, H. Fang, X. Zhang, and Q. Wang, "Data-Mined Continuous Hip-Knee Coordination Mapping With Motion Lag for Lower-Limb Prosthesis Control," *IEEE Transactions on Neural Systems and Rehabilitation Engineering,* vol. 30, pp. 1557-1566, 2022, doi: 10.1109/TNSRE.2022.3179978.

[24] A. Mai and S. Commuri, "Intelligent control of a prosthetic ankle joint using gait recognition," *Control Engineering Practice,* vol. 49, pp. 1-13, 2016, doi: https://doi.org/10.1016/j.conengprac.2016.01.004.

[25] Q. Li, T. Zhang, G. Li, Z. Li, H. Xia, and C. Y. Su, "Neural-Dynamics Optimization and Repetitive Learning Control for Robotic Leg Prostheses," *IEEE/ASME Transactions on Mechatronics,* vol. 27, no. 2, pp. 811-822, 2022, doi: 10.1109/TMECH.2021.3071936.

[26] J. Perry, "Gait Analysis: Normal and Pathological Function," (in eng), *Journal of Sports Science \& Medicine,* vol. 9, no. 2, pp. 353-353, Jun , day= 01 2010.

[27] G. Cicirelli, D. Impedovo, V. Dentamaro, R. Marani, G. Pirlo, and T. R. Orazio, "Human Gait Analysis in Neurodegenerative Diseases: A Review," *IEEE Journal of Biomedical and Health Informatics,* vol. 26, no. 1, pp. 229-242, 2022, doi: 10.1109/JBHI.2021.3092875.

[28] AposHeath. "An Introduction to Gait and Gait Abnormalities." https://www.aposhealth.com/blog/an-introduction-to-gait-and-gait-abnormalities/ (accessed.

[29] M. Myers and B. J. Chauvin, *Above the Knee Amputations*. StatPearls Publishing LLC, 2022.

[30] H. Crane, G. Boam, D. Carradice, N. Vanicek, M. Twiddy, and G. E. Smith, "Through-knee versus above-knee amputation for vascular and non-vascular major lower limb amputations," *Cochrane Database of Systematic Reviews,* no. 12, 2021, doi: 10.1002/14651858.CD013839.pub2.

[31] A. D. Knight, C. L. Dearth, and B. D. Hendershot, "Deleterious musculoskeletal conditions secondary to lower limb loss: considerations for prosthesis-related factors," *Advances in wound care,* vol. 10, no. 12, pp. 671-684, 2021.

[32] R. Baumgartner, "Oberschenkelamputation. Transfemorale Amputation [Upper leg amputation. Transfemoral amputation]." *Oper Orthop Traumatol.,* vol. 23, (4) pp. 296-305, 2011, doi: 10.1007/s00064-011-0039-5. .

[33] J. Geertzen *et al.*, "Dutch evidence-based guidelines for amputation and prosthetics of the lower extremity: Amputation surgery and postoperative management.," *Prosthet Orthot Int. ,* vol. Part 1., no. 39(5), pp. 351-60, 2015 doi: 10.1177/0309364614541460.

[34] J. H. B. Geertzen, S. M. van der Schans, P. C. Jutte, J. Kraeima, E. Otten, and R. Dekker, "Myodesis or myoplasty in trans-femoral amputations. What is the best option? An explorative study," *Medical Hypotheses,* vol. 124, pp. 7-12, 2019, doi: https://doi.org/10.1016/j.mehy.2019.01.008.

[35] K. Ahmed, "ITAP: Clinical outcomes and implant design optimisation using numerical modelling," 2021.

[36] M. Gonzalez-Fernandez. "Amputation: Recovery and Rehabilitation." https://www.hopkinsmedicine.org/health/treatment-tests-and-therapies/amputation/amputation-recovery-and-rehabilitation#:~:text=If%20the%20prosthesis%20is%20a,begin%20to%20use%20your%20prosthetic. (accessed.

[37] K. Hagberg, R. Brånemark, B. Gunterberg, and B. Rydevik, "Osseointegrated trans-femoral amputation prostheses: Prospective results of general and condition-specific quality of life in 18 patients at 2-year follow-up," *Prosthetics and Orthotics International,* vol. 32, no. 1, pp. 29-41, 2008, doi: 10.1080/03093640701553922.

[38] P. T. Pospiech, R. Wendlandt, H. H. Aschoff, S. Ziegert, and A. P. Schulz, "Quality of life of persons with transfemoral amputation: Comparison of socket prostheses and osseointegrated prostheses," *Prosthetics and Orthotics International,* vol. 45, no. 1, pp. 20-25, 2021, doi: 10.1177/0309364620948649.

[39] B. P. Kotamraju, S. Commuri, A. Mai, C. P. Dionne, J. Day, and W. J. J. Ertl, "Residuum Muscle Activation During Gait in Individuals with Traditional and Osteomyoplastic Amputation," *JPO: Journal of Prosthetics and Orthotics,* vol. 30, no. 4, pp. 207-213, 2018, doi: 10.1097/jpo.0000000000000207.

[40] A. Mai, S. Commuri, C. P. Dionne, J. Day, W. J. J. Ertl, and J. L. Regens, "Residual Muscle Contraction and Residuum Socket Interface Force in Men with Transtibial Osteomyoplastic Amputation," *JPO: Journal of Prosthetics and Orthotics,* vol. 25, no. 3, pp. 151-158, 2013, doi: 10.1097/JPO.0b013e31829a965c.

[41] C. Ertl, "The Ertl osteomyoplastic amputation: history, philosophy, misconceptions, misapplications," *Advancing Orthot Prosthet Care,* vol. 6, no. 2, 2010.

[42] M. Pouyan *et al.*, "Differences in muscle synergies between healthy subjects and transfemoral amputees during normal transient-state walking speed," *Gait & Posture,* vol. 76, pp. 98-103, 2020, doi: https://doi.org/10.1016/j.gaitpost.2019.10.034.

[43] Z. Kibria, B. P. Kotamraju, and S. Commuri, "An Intelligent Control Approach for Reduction of Gait Asymmetry in Transfemoral Amputees," presented at the International Symposium on Medical Robotics, Atlanta, Georgia, 2023. [Online]. Available: 10.1109/ISMR57123.2023.10130204.

[44] F. Davie-Smith, L. Paul, N. Nicholls, W. P. Stuart, and B. Kennon, "The impact of gender, level of amputation and diabetes on prosthetic fit rates following major lower extremity amputation," *Prosthetics and Orthotics International,* vol. 41, no. 1, pp. 19-25, 2017, doi: 10.1177/0309364616628341.

[45] H. Hobara *et al.*, "Biomechanical determinants of top running speeds in para-athletes with unilateral transfemoral amputation," *Prosthetics and Orthotics International,* vol. 47, no. 3, pp. 253-257, 2023, doi: 10.1097/pxr.0000000000000175.

[46] A. Pantall and D. Ewins, "Muscle activity during stance phase of walking: comparison of males with transfemoral amputation with osseointegrated fixations to nondisabled male volunteers," *Journal of Rehabilitation Research & Development,* vol. 50, no. 4, 2013.

[47] P. T. Pospiech, R. Wendlandt, H.-H. Aschoff, S. Ziegert, and A. P. Schulz, "Quality of life of persons with transfemoral amputation: Comparison of socket prostheses and osseointegrated prostheses," *Prosthetics and Orthotics International,* vol. 45, no. 1, pp. 20-25, 2021, doi: 10.1177/0309364620948649.

[48] E. C. Wentink, E. C. Prinsen, J. S. Rietman, and P. H. Veltink, "Comparison of muscle activity patterns of transfemoral amputees and control subjects during walking," *Journal of NeuroEngineering and Rehabilitation,* vol. 10, no. 1, p. 87, Aug , day= 02 2013, doi: 10.1186/1743-0003-10-87.

[49] X. Wang, Q. Meng, S. Bai, Q. Meng, and H. Yu, "Hybrid Active--Passive Prosthetic Knee: A Gait Kinematics and Muscle Activity Comparison with Mechanical and Microprocessor-Controlled Passive Prostheses," *Journal of Bionic Engineering,* vol. 20, no. 1, pp. 119-135, Jan , day= 01 2023, doi: 10.1007/s42235-022-00267-0.

[50] N. Bevacqua, G. D. Elce, and L. Intelangelo, "Assessing muscle strength of persons with transfemoral amputation with and without a prosthesis: A cross-sectional study," *Prosthetics and Orthotics International,* vol. 47, no. 5, pp. 532-536, 2023.

[51] R. Sinha, W. J. van den Heuvel, and P. Arokiasamy, "Adjustments to amputation and an artificial limb in lower limb amputees," *Prosthetics and Orthotics International,* vol. 38, no. 2, pp. 115-121, 2014, doi: 10.1177/0309364613489332.

[52] J. Liang *et al.*, "The effect of anti-gravity treadmill training for knee osteoarthritis rehabilitation on joint pain, gait, and EMG: Case report," *Medicine,* vol. 98, no. 18, p. e15386, 2019, doi: 10.1097/md.0000000000015386.

[53] S. Rashid *et al.*, "Muscle activation patterns around knee following neuromuscular training in patients with knee osteoarthritis: secondary analysis of a randomized clinical trial Open Access," *Archives of Physiotherapy,* vol. 2022, 07 2022, doi: 10.1186/s40945-022-00140-7.

[54] A. Pouya, M. D. Elysia, O. Jereme, H. M. Ross, B. Scott, and L. Janie, "High tibiofemoral contact and muscle forces during gait are associated with radiographic knee OA progression over 3 years," *The Knee,* vol. 41, pp. 245-256, 2023, doi: https://doi.org/10.1016/j.knee.2023.01.012.

[55] K. J. Bennett *et al.*, "EMG-Informed Neuromusculoskeletal Models Accurately Predict Knee Loading Measured Using Instrumented Implants," *IEEE Transactions on Biomedical Engineering,* vol. 69, no. 7, pp. 2268-2275, 2022, doi: 10.1109/TBME.2022.3141067.

[56] A. Rutkowska-Kucharska, M. Kowal, and S. Winiarski, "Relationship between Asymmetry of Gait and Muscle Torque in Patients after Unilateral Transfemoral Amputation," (in eng), *Applied bionics and biomechanics,* vol. 2018, pp. 5190816-5190816, Mar , day= 19 2018, doi: 10.1155/2018/5190816.

[57] D. A. Winter, *The biomechanics and motor control and human movement, Appendix A: Kinematic, Kinetic, and Energy Data*. John Wiley and Sons Ltd, 2009, pp. 296-360.

[58] I. The MathWorks, "MATLAB version: 9.13.0 (R2022b)," 2022.

[59] R. J. Schilling, J. J. Carroll, and A. F. Al-Ajlouni, "Approximation of nonlinear systems with radial basis function neural networks," *IEEE Transactions on Neural Networks,* vol. 12, no. 1, pp. 1-15, 2001, doi: 10.1109/72.896792.

[60] A. Ranavolo *et al.*, "Lower-Limb Joint Coordination Pattern in Obese Subjects," *BioMed Research International,* Dec 2012.

[61] D. A. Winter, *Kinematics*. John Wiley and Sons Ltd, 2009, pp. 45-81.

[62] D. A. Winter, *Biomechanics and motor control of human movement*, 4 ed. Hoboken, N.J.: Wiley, 2009, p. 370.

[63] A. Mai and S. Commuri, "Intelligent Control of a Prosthetic Ankle Joint," presented at the International Conference on Informatics in Control, Automation and Robotics, 2013. [Online]. Available: https://www.scitepress.org/Papers/2013/44856/pdf/index.html.

[64] F. M. L. Amirouche, *Computational Methods in Multibody Dynamics*. Englewood Cliffs, NJ: Prentice Hall, 1992.

[65] A. Mai, S. Commuri, C. P. Dionne, J. Day, W. J. J. Ertl, and J. L. Regens, "Effect of Prosthetic Foot on Residuum-Socket Interface Pressure and Gait Characteristics in an Otherwise Healthy Man With Transtibial Osteomyoplastic Amputation," *JPO: Journal of Prosthetics and Orthotics,* vol. 24, no. 4, 2012.

[66] M. Peasgood, E. Kubica, and J. McPhee, "Stabilization of a Dynamic Walking Gait Simulation," *Journal of Computational and Nonlinear Dynamics,* vol. 2, no. 1, pp. 65-72, 2006, doi: 10.1115/1.2389230.

[67] M. Ackermann and A. J. Bogert, "Optimality principles for model-based prediction of human gait," *Journal of Biomechanics,* vol. 43, no. 6, pp. 1055-1060, 2010, doi: https://doi.org/10.1016/j.jbiomech.2009.12.012.

[68] R. K. Kenton, F. Serena, and A. F. Carlo, "Gait asymmetry of transfemoral amputees using mechanical and microprocessor-controlled prosthetic knees," *Clinical*

Biomechanics, vol. 27, no. 5, pp. 460-465, 2012, doi: https://doi.org/10.1016/j.clinbiomech.2011.11.011.

[69] Y. Feng, C. Mao, W. Zhang, and Q. Wang, "Gait-Symmetry-Based Human-in-the-Loop Optimization for Unilateral Transtibial Amputees With Robotic Prostheses," *IEEE Transactions on Medical Robotics and Bionics,* vol. 4, no. 3, pp. 744-753, 2022, doi: 10.1109/TMRB.2022.3176476.

[70] Z. Kibria and S. Commuri, "Neuro-dynamic Control of an above Knee Prosthetic Leg," in *Proceedings of the 19th International Conference on Informatics in Control, Automation and Robotics - ICINCO,*, 2022, pp. 29-37, doi: 10.5220/0011268200003271. [Online]. Available: https://www.scitepress.org/PublicationsDetail.aspx?ID=Gy1OKsCjNEI=&t=1

[71] X. Zhou, J. Chen, G. Chen, Z. Zhao, and Y. Zhao, "Anthropometric body modeling based on orthogonal-view images," *International Journal of Industrial Ergonomics,* vol. 53, pp. 27-36, 2016, doi: https://doi.org/10.1016/j.ergon.2015.10.007.

[72] M. Myers and B. Chauvin, "Above the Knee Amputations," ed. Florida: StatPearls Publishing, 2021.

[73] H. P. Ryan, C. Husted, and M. D. Lewek, "Improving Spatiotemporal Gait Asymmetry Has Limited Functional Benefit for Individuals Poststroke," *Journal of Neurologic Physical Therapy,* vol. 44, no. 3, pp. 197-204, 2020, doi: 10.1097/npt.0000000000000321.

[74] W. Pirker and R. Katzenschlager, "Gait disorders in adults and the elderly," *Wiener klinische Wochenschrift,* vol. 129, no. 3, pp. 81-95, Feb , day= 01 2017, doi: 10.1007/s00508-016-1096-4.

[75] M. M. Mielke *et al.*, "Assessing the Temporal Relationship Between Cognition and Gait: Slow Gait Predicts Cognitive Decline in the Mayo Clinic Study of Aging," *The Journals of Gerontology: Series A,* vol. 68, no. 8, pp. 929-937, 2012, doi: 10.1093/gerona/gls256.

[76] R. Versluys, P. Beyl, M. V. Damme, A. Desomer, R. V. Ham, and L. Dirk, "Prosthetic feet: State-of-the-art review and the importance of mimicking human ankle–foot biomechanics," *Disability and Rehabilitation: Assistive Technology,* vol. 4, no. 2, pp. 65-75 , year = 2009, 2009, doi: 10.1080/17483100802715092.

[77] S. G. Bhat, S. Redkar, and T. G. Sugar, "Development of a Passive Prosthetic Ankle With Slope Adapting Capabilities," in *ASME 2018 International Mechanical Engineering Congress and Exposition*, 2018, vol. Volume 3: Biomedical and Biotechnology Engineering, V003T04A018, doi: 10.1115/imece2018-86593. [Online]. Available: https://doi.org/10.1115/IMECE2018-86593

[78] M. E. Carney, T. Shu, R. Stolyarov, J.-F. Duval, and H. M. Herr, "Design and Preliminary Results of a Reaction Force Series Elastic Actuator for Bionic Knee and Ankle Prostheses," *IEEE Transactions on Medical Robotics and Bionics,* vol. 3, no. 3, pp. 542-553, 2021, doi: 10.1109/TMRB.2021.3098921.

[79] A. Fleming, H. Stephanie, B. Elizabeth, H. Frank, and H. H. Helen, "Direct continuous electromyographic control of a powered prosthetic ankle for improved postural control after guided physical training: A case study," *Wearable Technologies,* vol. 2, p. e3, 2021, doi: 10.1017/wtc.2021.2.

[80] R. Stolyarov, M. Carney, and H. Herr, "Accurate Heuristic Terrain Prediction in Powered Lower-Limb Prostheses Using Onboard Sensors," *IEEE Transactions on Biomedical Engineering,* vol. 68, no. 2, pp. 384-392, 2021, doi: 10.1109/TBME.2020.2994152.

[81] M. Windrich, M. Grimmer, O. Christ, S. Rinderknecht, and P. Beckerle, "Active lower limb prosthetics: a systematic review of design issues and solutions," *BioMedical Engineering OnLine,* vol. 15, no. 3, p. 140, Dec , day= 19 2016, doi: 10.1186/s12938-016-0284-9.

[82] Y. Wen, J. Si, X. Gao, S. Huang, and H. H. Huang, "A New Powered Lower Limb Prosthesis Control Framework Based on Adaptive Dynamic Programming," *IEEE Transactions on Neural Networks and Learning Systems,* vol. 28, no. 9, pp. 2215-2220, 2017, doi: 10.1109/TNNLS.2016.2584559.

[83] C. Lu, J. Si, and X. Xie, "Direct heuristic dynamic programming for damping oscillations in a large power system," (in "English (US)"), *IEEE Transactions on Systems, Man, and Cybernetics, Part B: Cybernetics,* vol. 38, no. 4 ,, pp. 1008--1013, aug 2008, doi: 10.1109/TSMCB.2008.923157.

[84] M. K. Bugeja and S. G. Fabri, "Neuro-adaptive dynamic control for mobile robots: Experimental validation," presented at the 2008 3rd International Symposium on Communications, Control and Signal Processing, Saint Julian's, Malta, 2008.

[85] S. M. N. Mahmud, S. A. Nivison, Z. I. Bell, and R. Kamalapurkar, "Safe Model-Based Reinforcement Learning for Systems With Parametric Uncertainties," (in English), *Frontiers in Robotics and AI,* Original Research vol. 8, 2021-December-16 2021, doi: 10.3389/frobt.2021.733104.

[86] D. Bertsekas and J. Tsitsiklis, "Neuro-dynamic programming : an overview," presented at the Proceedings of 1995 34th IEEE Conference on Decision and Control, New Orleans, LA, USA, 1995.

[87] T. Chen, A. Babanin, A. Muhammad, B. Chapron, and C. Chen, "Modified Evolved Bat Algorithm of Fuzzy Optimal Control for Complex Nonlinear Systems," *ROMANIAN JOURNAL OF INFORMATION*

SCIENCE AND TECHNOLOGY, vol. 23, pp. 28-40, 2020.

[88] G. Rigatos, P. Siano, D. Selisteanu, and R. E. Precup, "Nonlinear Optimal Control of Oxygen and Carbon Dioxide Levels in Blood," *Intelligent Industrial Systems,* vol. 3, no. 2, pp. 61-75, Jun , day= 01 2017, doi: 10.1007/s40903-016-0060-y.

[89] I. Alexandru Zamfirache, R.-E. Precup, R.-C. Roman, and M. P. Emil, "Policy Iteration Reinforcement Learning-based control using a Grey Wolf Optimizer algorithm," *Information Sciences,* vol. 585, pp. 162-175, 2022, doi: https://doi.org/10.1016/j.ins.2021.11.051.

[90] E. Soares, P. Angelov, B. Costa, M. Castro, S. Nageshrao, and D. Filev, "Explaining Deep Learning Models Through Rule-Based Approximation and Visualization," *IEEE Transactions on Fuzzy Systems,* 05 2020, doi: 10.1109/TFUZZ.2020.2999776.

[91] D. A. Winter, *The Biomechanics and Motor Control of Human Gait*. University of Waterloo Press, 1987.

[92] A. Forner-Cordero, H. J. F. M. Koopman, and F.C.T, "Describing gait as a sequence of states," *Journal of Biomechanics,* vol. 39, no. 5, pp. 948-957, 2006, doi: https://doi.org/10.1016/j.jbiomech.2005.01.019.

[93] S. Turner, A. Belsi, and A. H. McGregor, "Issues faced by people with amputation(s) during lower limb prosthetic rehabilitation: A thematic analysis," *Prosthetics and Orthotics International,* vol. 46, no. 1, pp. 61-67, 2022, doi: 10.1097/pxr.0000000000000070.

[94] A. Brandt and H. Huang, "Effects of extended stance time on a powered knee prosthesis and gait symmetry on the lateral control of balance during walking in individuals with

unilateral amputation," *Journal of NeuroEngineering and Rehabilitation,* vol. 16, no. 1, p. 151, Nov , day= 29 2019, doi: 10.1186/s12984-019-0625-6.

[95] P. Leva, "Adjustments to Zatsiorsky-Seluyanov's segment inertia parameters," *Journal of Biomechanics,* vol. 29, no. 9, pp. 1223-1230, 1996, doi: https://doi.org/10.1016/0021-9290(95)00178-6.